수의학 석사학위 논문

신경세포에서 부티르산에 의한 NOX2 억제와 Nrf2 안정화를 통한 고콜레스테롤 유도성 아밀로이드 생성 억제 효과

Inhibitory effect of sodium butyrate on high cholesterol-induced amyloidogenesis through NOX2 suppression and Nrf2 stabilization in neuronal cells

2020년 2월

지도교수: 한 호 재

서울대학교 대학원

수의학과 수의생명과학 전공
(수의생리학)

김 서 일

신경세포에서 부티르산에 의한 NOX2 억제와 Nrf2 안정화를 통한 고콜레스테롤 유도성 아밀로이드 생성 억제 효과

Inhibitory effect of sodium butyrate on high cholesterol-induced amyloidogenesis through NOX2 suppression and Nrf2 stabilization in neuronal cells

지도교수 한 호 재

이 논문을 수의학 석사 학위논문으로 제출함

2019년 11월

서울대학교 대학원

수의학과 수의생명과학 전공

(수의생리학)

김 서 일

김서일의 수의학 석사 학위논문을 인준함

2019년 12월

위 원 장 이 장 헌 (인)

부위원장 한 호 재 (인)

위 원 성 제 경 (인)

ABSTRACT

Inhibitory effect of sodium butyrate on high cholesterol-induced amyloidogenesis through NOX2 suppression and Nrf2 stabilization in neuronal cells

Seo Yihl Kim

Major in Veterinary Biomedical Science

Department of Veterinary Medicine

The Graduate School

Seoul National University

The gut microbiota dysbiosis occurs in many obese patients, which includes butyrate-producing bacteria are reduced. Although sodium butyrate (NaB) has emerged as the potential therapeutic substance in Alzheimer's disease (AD), there is a lack of detailed

results into what signaling pathways affect amyloidogenesis in AD induced by obesity. Thus, the study investigated the regulatory role of NaB on β-site amyloid precursor protein cleaving enzyme 1 (BACE1)-dependent amyloidogenesis in neuronal cells under high cholesterol conditions. In these results, it was verified that the microbial diversity of obese mice was much reduced compared to that of normal mice, and the concentration of NaB in the plasma of obese mice was also reduced. It was also observed that reactive oxygen species (ROS) were overproduced because of increased NADPH oxidase 2 (NOX2) expression levels in SK-N-MC cells under high cholesterol conditions. Meanwhile, NaB decreased the expression levels of NOX2, which in turn prevented the overproduction of ROS, ultimately inhibiting BACE1 expression and amyloid beta peptide (Aβ) accumulation caused by high cholesterol. In addition, the increase in p21 levels was induced by increasing the nuclear translocation of specific protein 1 (sp1) due to the acetylation regulation of sp1 by NaB. NaB increased the expression levels of p21 in SK-N-MC cells that were exposed to high cholesterol environment, which contributes to p21/nuclear factor erythroid 2-related factor 2 (Nrf2) co-localization. This leads Nrf2 stabilization to facilitate the nuclear translocation of Nrf2. In conclusion, it was demonstrated that NaB prevents NOX2-dependent ROS production via NOX2 downregulation and eliminates excessive ROS through antioxidant enzymes upregulation by the

p21/Nrf2 pathway, which is critical for inhibiting BACE1-dependent amyloidogenesis in neuronal cells exposed to high cholesterol environment.

Keywords: Sodium butyrate, Neuronal cells, Amyloidogenesis, Cholesterol, Reactive oxygen species

Student Number: 2017-29949

CONTENTS

LIST OF FIGURES

ABBREVIATIONS

HFD	High fat diet
ND	Normal diet
AD	Alzheimer's disease
Aβ	Amyloid β peptide
APP	Amyloid precursor protein
BACE1	Beta-site amyloid precursor protein cleaving enzyme 1
PSEN1	Presenilin-1
NaB	Sodium butyrate
NaP	Sodium propionate
NaA	Sodium acetate
ROS	Reactive oxygen species
CNS	Central nervous system
SCFAs	Short chain fatty acids
HDAC	Histone deacetylase
GPCR	G-protein coupled receptor
NOX	NADPH oxidase

NF-κB	Nuclear factor-kappa B
mtROS	Mitochondrial ROS
SOD	Superoxide dismutase
GPX	Glutathione peroxidase
Sp1	Specific protein 1
Nrf2	Nuclear factor erythroid 2-related factor 2
GC-MS	Gas chromatography-mass spectrometry
ELISA	Enzyme-linked immunosorbent assay
NAC	N-Acetylcysteine

INTRODUCTION

Accumulating studies have shown that the meta-analysis of gut microbiota composition in obese patients showed that butyrate-producing bacteria are reduced in the gut (Jakobsdottir et al., 2013; Lu et al., 2016). In previous studies, NaB was already proposed as a therapeutic substance for AD through antioxidant and anti-inflammatory functions (Canani et al., 2011; Govindarajan et al., 2011). However, there are few studies on how the mechanism of NaB regulates obesity-induced AD. Therefore, it can be said that the study of how NaB affects amyloidogenesis caused by obesity is meaningful.

One of the typical characteristics found in obese patients is high cholesterol level, which is also a major cause of the pathogenesis of AD (Alford et al., 2018; Kivipelto et al., 2006; Klop et al., 2013). Cholesterol affects the synthesis, elimination, aggregation, and neurotoxicity of Aβ, a representative marker of AD (Sun et al., 2015). When cells are exposed to high cholesterol environment, they generally produce excessive ROS (Wang et al., 2017). Neurons under high cholesterol conditions also produce excessive ROS, which is well known as one of the major contributors to amyloidogenesis (Sun et al., 2015). There are generally two types

of ROS production sources in the cells; one is NOX and the other is the mitochondria (Bae et al., 2011). Previous studies reported that the critical factor of ROS in the central nervous system (CNS) is NOX (Nayernia et al., 2014), but further studies are needed to determine the specific source of excessive ROS produced in neuronal cells exposed to high cholesterol environment. As it has not been reported how to produce excessive ROS in neurons under high cholesterol conditions, it will be possible that verifying the major source of excessive ROS can be a key factor in high cholesterol-induced Aβ accumulation. Thus, it is essential to investigate how NaB affects the cell signaling pathway-associated NOX or mitochondrial ROS (mtROS) production. As the mechanisms by which NaB inhibits ROS production in neurons exposed to high cholesterol environment are not fully understood, these mechanisms will help to further understand the antioxidant effect of NaB. Furthermore, these mechanisms may also be key mechanisms for the inhibitory effect of NaB on Aβ accumulation induced by high cholesterol.

The proper balance of histone acetyltransferases (HATs) and histone deacetylases (HDACs) regulates the acetylation of histone or transcription factors. NaB is a well - known HDAC inhibitor, so regulates gene expression in a variety of ways through HDAC inhibitor function (Davie. 2003). The regulation of transcription

factor activity through acetylation may increase or decrease activity of each transcription factor (Chueh et al., 2015). Therefore, since the transcription factor activity varies according to cell type and condition, many experiments and further studies are needed. Studies targeting HDAC inhibitors as a therapeutic strategy for AD have been preceded. The Studies have shown that many HDAC inhibitors, including NaB, protected cognitive impairment and inhibit Aβ generation in AD patients (Xu et al., 2011). However, it is not known what mechanism of NaB as HDAC inhibitors blocks the development of AD in neurons.

The most prominent transcription factor that regulates the expression of antioxidant enzymes, such as superoxide dismutase (SOD), catalase, and glutathione peroxidase (GPX) is Nrf2 (David et al., 2017). In response to oxidative damages, cells are protected by the Nrf2/Keap1/ARE antioxidant pathway (David et al., 2017; Hayes et al., 2014). However, several studies reported that overproduced ROS in response to oxidative damages make the antioxidant defense of cells vulnerable (Matough et al., 2012). However, the antioxidant activity of NaB is one of the representative functions of NaB which modulates the expression levels of antioxidant enzymes. Although NaB has been shown to act as an activator of Nrf2 to regulate antioxidant enzymes (Dong et al., 2017), the specific mechanisms by which NaB activates Nrf2 under

high cholesterol conditions have not yet been elucidated. Previous studies reported that NaB increases the expression levels of p21 which stabilizes Nrf2 by binding to Nrf2 (Chen et al., 2009; Crim et al., 2008). Therefore, it seems necessary to investigate the mechanisms by which NaB stabilizes Nrf2 by increasing the p21/Nrf2 pathway.

In the present study, a high fat diet (HFD)-induced obese mice model was prepared for AD caused by obesity. To investigate the exact mechanisms of the inhibitory effect of NaB on amyloidogenesis, SK-N-MC cells which are a human neuronal epithelioma cell line were used (Waheed Roomi et al., 2013). SK-N-MC cells were treated with high cholesterol or NaB for the study. To address this issue, the study identified that the specific mechanisms of how NaB inhibits high cholesterol-induced excessive ROS and investigated the protective role of NaB against Aβ accumulation caused by high cholesterol.

MATERIALS AND METHODS

1. Materials

The human neuroblastoma cell line SK-N-MC was acquired from Korean Cell Line Bank (Seoul, Korea). Fetal bovine serum (FBS) and Dulbecco's modified eagle medium (DMEM) were purchased from Hyclone (Logan, UT, USA). Antibiotics and serum replacement (SR) were acquired from Gibco (Grand Island, NY, USA). The antibodies of β-Actin (sc-47778), Lamin A/C (sc-376248), GPX4 (sc-166570), catalase (sc-271803), NF-κB (sc-8008), BACE1 (sc-33711), and PSEN1 (sc-365450) were purchased from Santa Cruz Biotechnology (Santa Cruz, CA, USA). The antibodies of APP (ab32136), BACE1 (ab2077), sp1 (ab227383), Nrf2 (ab89443), and Aβ (ab2530) were purchased from Abcam (Cambridge, England). The antibody of NOX2 (611414) was purchased from BD bioscience. The antibody of SOD1 (CSB-PA02864A0Rb) was purchased from CusaBio (Houston, TX, USA) and SOD2 (06-984) was purchased from EMD Millipore (Burlington, MA, USA). The antibodies of p53 (PA5-27822) and p21 (MA5-14949) were purchased from Thermo Fisher and TurboFect, human or mouse Aβ (1-42) ELISA kit, CM-H2DCFDA,

MitoSOX™ Red, and RNAlater™ solution were also obtained from Thermo Fisher (Waltham, MA, USA). ATN-224 was purchased from CSNpharm and Bay11-7082 was purchased from Calbiochem. Paraformaldehyde (PFA) was purchased from Lugen (Bucheon, Korea). EzSubcell™ subcellular fractionation kit was acquired from Atto (Tokyo, Japan). Sodium acetate was purchased from FUJIFILM Wako Pure Chemical Corporation. NAC, Vas2870, mitotempo, sodium butyrate, sodium propionate, butyric acid, acrylic acid, m-phosphoric acid, propyl formate, cholesterol-water soluble, DAPI, Triton X-100, ibuprofen, and pertussis toxin were purchased from Sigma Chemical Company (St. Louis, MO, USA). mRNA primers for APP, BACE1, PSEN1, NOX1, NOX2, NOX3, NOX4, SOD1, SOD2, catalase, GPX4, and ACTB were purchased from Cosmo Genetech (Seoul, Korea). Nrf2 siRNA and SMCT1 siRNA were acquired from Bioneer (Daejeon, Korea). NT siRNA was purchased from Dharmacon (Lafayette, CO, USA).

2. Culture of SK-N-MC cells

SK-N-MC cells were cultured without a feeder layer in high-glucose Dulbecco's Modified Eagle Medium (DMEM), supplemented with 10% FBS and 1% antibiotic-antimycotic solution at 37℃ with 5% CO_2. Cells were grown in 60 or 100mm

diameter culture dishes, or 12 or 96well plates in an incubator maintained at 37℃ with 5% CO_2. When the cells reach approximately 60% confluency, the medium was replaced with DMEM supplemented with 1% antibiotic-antimycotic solution and 2% of SR 24h before the experiments. Cells were maintained in 2% SR in DMEM containing 1% antibiotics and agents such as cholesterol, NaB, and ibuprofen.

3. Preparation of brain tissue of the HFD-induced obese mouse model

To induce obesity through a diet, six-week-old male ICR mice were fed either a regular chow diet or a HFD (Rodent Diet with 60kcal% Fat and 90g Added NaCl /4,057 kcal, Research Diets Inc., New Brunswick, NJ, USA) for 14weeks. Mice were stabilized in the new environment for 3days before experimentation. Mice were granted *ad libitum* access to food and water. The room was maintained under standard environmental conditions (24 ± 2℃, 12/12h light/dark cycle with lights on at 07:00). Mice were randomly assigned. The experiments were performed according to the "Guide for Animal Experiments" (Edited by the Korean Academy of Medical Sciences) and approved by the Institutional Animal Care

and Use Committee (IACUC) of Seoul National University (SNU-180802-2). The brains were removed and post-fixed by 4% paraformaldehyde in 0.1M PBS for 12h. The brain tissues were cryo-protected by overnight infusion with 90% sucrose, and 30㎛-thick coronal sections were serially cut using a cryostat (Leica, Deerfield, Germany). The sections were transferred to 6well plates containing PBS for further processing.

4. Metagenomic 16S rRNA sequencing and data analysis

Mouse fecal samples were stored in RNAlater™ solution at −80℃ until processing. DNA extractions for 16S rRNA analysis were performed by using FastDNA® SPIN Kit for Soil (MP Biomedicals, Solon, CA, USA) based on manufacturer's recommendations. The bacterial 16S rRNA V3-V4 region was amplified in accordance with the Illumina 16S Metagenomic Sequencing Library Preparation guide (Illumina, CA, USA), using the primers with added adapter overhang sequences (Klindworth et al., 2013): forward primer: 5'-TCGTCGGCAGCGTCAGATGT GTATAAGAGACAGCCTACGGGNGGCWGCAG -3', reverse primer: 5'-GTCTCGTGGGCTCGGAGATGTGTATAAGAGACAGGACTACHVGGGTA

TCTAATCC −3'. Also, the MiSeq platform (Illumina, CA, USA) with the 2 × 300bp paired−end sequencing was used for amplicon sequencing through standard Illumina sequencing protocols. A quality control for the raw sequences of each sample was examined using FastQC (Davis et al., 2013). Then, QIIME2 (v.2019.4) (Bolyen et al., 2019), a standardized pipeline for 16S rRNA sequencing data was processed. The q2−cutadapt plugin (Martin. 2011) was used for removing the primer sequences and the DADA2 software package (Callahan et al., 2016) wrapped in QIIME2 was used to quality control including quality filtering, denoising, and used to feature table construction containing amplicon sequence variants (ASVs). After that, the q2−phylogeny plugin was used for generating the phylogenetic tree. Furthermore, alpha diversity (α−diversity) and beta diversity (β−diversity) were performed as the core−metrics−phylogenetic in the QIIME2 diversity plugin provides these two types of diversity analysis. For taxonomic annotation, the QIIME2 feature−classifier plugin (classify−sklearn) with a pre−trained Naïve Bayes classifier on the GreenGene database [v.13_8 with 99% similarity operational taxonomic units (OTUs)] (DeSantis et al., 2006) was performed. Finally, the Statistical Analysis of Metagenomic Profiles (STAMP) software (Parks et al., 2014) was used for comparing the taxonomic profiling analysis between groups.

5. Preparation of plasma samples

All procedures for preparation of samples were performed following the previous report (Skoglund. 2016). A hundred μL of internal standard solution (150 μM acrylic acid, 1,500 μM m-phosphoric acid) was added to 200 μL plasma. Samples were vortexed for 5min followed by centrifugation (30min, 14,916rpm) and left to solidify the precipitate for 30min at 4℃. A hundred μL of the clear supernatant was transferred into a new tube and 100 μL washed propyl formate was added. Samples were vortexed for 5min followed by centrifugation (10min, 14,916rpm) before transferring 50 μL of the organic layer into GC vials (Waters, Milford, Massachusetts, United States) for analysis.

6. GC-MS analysis

One μL sample was injected into a straight glass liner, held at 200℃. Helium (1mL/min) was used as carrier gas in TR-FAME (25m × 0.32mm × 0.25μm). The initial oven temperature of 60℃ was maintained for 4min, then ramped to 130℃ at 50℃/min and held for 3.7min and finally raised to 240℃ at 30℃/min and held for 10min. The transfer line and ion source

temperature is 250℃. All samples, standards, and blanks were analyzed randomly at the GC-MS system. Trace 1300 Series gas chromatograph with TSQ Series mass spectrometer (Thermo Fisher, MA, USA) were used. Integrations were performed automatically with Triplus RSH autosampler (Thermo Fisher, MA, USA).

7. Western blot analysis

Cells were detached from the 60 or 100mm diameter culture dishes with a scraper and gathered by centrifugation (13,200 rpm, 4℃, 5min). Harvested cells and brain tissues were lysed by RIPA lysis buffer (ATTO Corporation, Tokyo, Japan) and incubated for 30min on ice. The lysates were then cleared by centrifugation (13,200rpm, 4℃, 30min). The protein concentration was measured by the bicinchoninic acid (BCA) assay kit (Bio-Rad, Hercules, CA, USA). Samples containing 10 ug of protein were prepared for 8-15% sodium dodecyl sulfate polyacrylamide gel electrophoresis (SDS-PAGE) and then transferred to a polyvinylidene fluoride (PVDF) membrane and blocked with 5% skim milk (Gibco) dissolved in TBST for 40min. The blocked membranes were washed with TBST and incubated with primary antibody overnight at 4℃. The membranes were

subsequently washed and incubated with HRP-conjugated secondary antibody at room temperature for 2h. The western blotting bands were visualized by means of chemiluminescence (Bio-Rad,Hercules, CA, USA). Specific bands were detected using a ChemiDoc™ XRS+ System (Bio-Rad, Hercules, CA, USA) and analyzed by using ImageJ software.

8. Reverse transcription-polymerase chain reaction (RT-PCR) and real-time PCR

RNA was extracted using MiniBEST Universal RNA Extraction Kit (TaKaRa, Otsu, Shinga, Japan). Reverse transcription was performed using 1 μg of RNA with a Maxime RT-PCR PreMix Kit (Intron Biotechnology, Seongnam, Korea) to obtain cDNA. Two microliters of cDNA were then amplified using Quanti NOVA SYBR Green PCR Kits (Qiagen, Hilden, Germany). Real-time quantification of RNA targets was performed in a Rotor-Gene 6000 realtime thermal cycling system (Corbett Research, NSW, Australia). The reaction mixture (20 μL) contained 200ng of total RNA, 0.5mM of each primer for the gene of interest, and appropriate amounts of enzymes and fluorescent dyes as recommended by the manufacturer. The real-time PCR was performed as follows: 15min at 95℃ for DNA polymerase

activation; 15sec at 95℃ for denaturing; and 50cycles of 15sec at 94℃, 30sec at 54℃, and 30sec at 72℃. Data were collected during the extension step, and analysis was performed using the software provided; melting curve analysis was performed to verify the specificity and identity of the PCR products. Normalization of gene expression levels was performed by using the ACTB gene as an endogenous control. Sequences of the primers used are described in Table 1.

Table 1. Sequences of primers used for PCR.

Gene	Identification	Sequence (5'–3')
APP	Forward	CTGGCTGAAGAAAGTGACAATG
	Reverse	TCCTCTACCTCATCACCATCCT
BACE1	Forward	GGAGTACAAAGACAGGGAATAG
	Reverse	GAATAAAGGGTGGTTCAGATAGA
PSEN1	Forward	AGGAAAGGGGAGTAAAACTTGG
	Reverse	AAAGGTGATGGAGATTGGAAGA
NOX1	Forward	TCCCAGCAGAAGGTTGTGATTACC
	Reverse	TGCCATTCCAGGAGAGAGATTGAG
NOX2	Forward	CTGCTCAACAAGAGTTCGAAGA
	Reverse	GCCTCCTTCAGGGTTCTTTATT
NOX3	Forward	ACAACATCACCTTCTGTAGAGACCG
	Reverse	AATCCATTTCCAAGCCGAGG
NOX4	Forward	GACTTTACAGGTATATCCGGAGCAA
	Reverse	TGCAGATACACTGGACAATGTAGA
SOD1	Forward	CAATTTCGAGCAGAAGGAAAGT
	Reverse	ACCGTGTTTTCTGGATAGAGGA
SOD2	Forward	ATGGTGGTGGTCATATCAATCA
	Reverse	TGTAAGTGTCCCCGTTCCTTAT
Catalase	Forward	GACCGAGAGAGAATTCCTGAGA
	Reverse	CGAGATCCCAGTTACCATCTTC
GPX4	Forward	CATGGTTAACCTGGACAAGTACC
	Reverse	GCAGATCTTGCTGAACATATCG
ACTB	Forward	AACCGCGAGAAGATGACC
	Reverse	AGCAGCCGTGGCCATCTC

9. Detection of intracellular ROS and mitochondrial ROS

The CM-H2DCFDA, MitoSOX™ Red were used to measure the intracellular ROS, mitochondrial ROS respectively. Cells were seeded in a 96well plate at same density (2×10^3 cells per well). Cells were treated with 5 μM DCF-DA or 2 μM MitoSOX™ Red and then incubated in an incubator at 37℃ with 5% CO_2 for 30min or 15min respectively. Cells were washed twice with PBS and then measured with a luminometer (Victor3; PerkinElmer Inc., Waltham, MA, USA). The fluorescence intensity of CM-H2DCFDA was measured with a luminometer at an excitation and emission wavelength of 485 and 535nm and those of MitoSOX™ Red were measured at an excitation and emission wavelength of 530 and 580nm.

10. Flow cytometry

Cells were seeded in 12well culture dishes. When cells were at 60% confluence, medium was replaced with 2% SR in DMEM containing 1% antibiotics for 24h. Cells were stained with 5 μM DCF-DA for 30min or 2 μM MitoSOX™ Red for 15min. Cells were washed with PBS two times and treated with a 0.05%

trypsin and 0.5mM EDTA solution to detach cells from the dish for 3min. Cells were centrifuged at 3,000rpm for 5min. DCF-DA or MitoSOX™ Red staining were determined via flow cytometry (CytoFlex; Beckman Coulter, Fullerton, CA,USA).

11. Nuclear Fractionation

To prepare the cytosolic and nuclear fractionized samples, the EzSubcell™ subcellular fractionation/extraction kit was used. All procedures of the subcellular fractionation assay followed manufacturer's protocol. Nuclear NF-κB, Nrf2, p53, and sp1 expression levels in nuclear fractionized samples were normalized by lamin A/C expression levels.

12. Immunocytochemistry

Cells were washed with PBS on a confocal dish. Cells were fixed with 4% paraformaldehyde (PFA) for 10min and then, incubated in 0.1% Triton X-100 for membrane permeabilization for 10min. Cells were incubated with 5% normal goat serum in PBS for 30min and with primary antibodies for overnight in 4℃. Next, Cells were washed with PBS three times and incubated

with Alexa Fluor™ 488 or 555-conjugated secondary antibodies for 2h at room temperature. Immunofluorescence images were obtained by a super-resolution radial fluctuations (SRRF) imaging system (Andor Technology, Belfast, UK) (Gustafsson et al., 2016).

13. Immunohistochemistry

Tissues were deparaffinized with xylene and 100, 95, 70, and 50% ethanol. For peroxide inactivation, the tissues were then incubated on 3% H_2O_2 in methanol and washed with PBS. For permeabilization, the tissues were incubated in PBS containing 0.5% Triton X-100 for 15min, washed with PBS, and incubated with 5% NGS in PBS for 30min. The tissues were labeled with 5% NGS in PBS containing APP, BACE1, and Aβ antibodies at a ratio of 1:100 for 2h, followed by secondary antibody and PI in 1:100 ratio for 1h at room temperature. After washing with PBS for 15min, images were obtained by using FluoView™ 300 confocal microscope (Olympus).

14. Aβ ELISA

The Aβ (1-42) concentration level in medium sample was measured by commercial enzyme-linked immunosorbent assay (ELISA) kits. Medium samples were collected and centrifugated at 13,200rpm for 5min and the supernatant samples were collected as ELISA samples. All procedures of the Aβ ELISA assay were performed according to the manufacturer's protocol.

15. Water soluble tetrazolium salt (WST-1) assay

WST-1 assay was used for determining cell proliferation and cell viability *in vitro* model. All procedures of the assay were conducted according to the manufacturer's protocol. Cells were seeded in 96well plate (2×10^3 cells per well). EZ-Cytox^{TM} reagent was added to each well and the cells were incubated for 1h in 5% CO_2 incubator at 37℃. The absorbance of each sample was measured at a wavelength of 450nm by using a microplate reader.

16. Trypan blue cell viability assay

The SK-N-MC cells were washed with PBS, and then incubate with a 0.05% trypsin and 0.5mM EDTA solution to detach the cells. Trypsin inhibitor (PBS with 10% FBS) was added to quench trypsin. Cell suspension solution was centrifugated 3,000rpm for 5min. Cell pellet was suspended with 0.4% trypan blue in PBS to stain the dead cells. 10 μL was dispensed on the cell counting chamber slides. Trypan blue stained or unstained cells were counted by using a Countess II FL (Thermo Fisher, MA, USA).

17. Statistical analysis

Quantitative data are presented as the mean ± standard error of mean (S.E.M). Statistical analysis was conducted by using GraphPad Prism Version 5.0 (GraphPad Inc., San Diego,CA, USA). Statistical differences between more than two groups were assessed using one-way analysis of variance (ANOVA) with a post hoc Bonferroni-Dunn test. The student's t-test was conducted for comparing the means of treatment groups with that of the control group. $p < 0.05$ was considered statistically significant.

RESULTS

1. Obesity induces BACE1 expression, Aβ accumulation, and the alteration of the gut microbiota composition in mice model

BACE1 expression and Aβ accumulation in the hippocampus and cortex were verified to confirm the effect of obesity. The mice fed a normal diet (ND) as control or a HFD every week for 14weeks were prepared. This study found that the expression levels of amyloid precursor protein (APP) and BACE1 were higher in HFD-fed mice than in ND-fed mice (Fig. 1A). In the immunohistochemistry results, APP, BACE1 and Aβ were also increased in the hippocampus and cortex regions in the brains of HFD-fed mice compared to ND-fed mice (Fig. 1B). These results indicated that HFD has an effect on increasing APP, BACE1 expression and Aβ accumulation in mice brain. The effect of HFD through 16S rRNA analysis, alpha and beta analysis was investigated by using fecal samples of mice. These analyses

showed that the gut microbiota diversity was significantly lower in HFD-fed mice than in ND-fed mice (Fig, 2A-B). Firmicutes to which most butyrate-producing bacteria belong in the phylum level were not altered in the HFD group compared to the ND group (Fig. 3A). Clostridiales to which most butyrate-producing bacteria belong in the order level were also not changed in the HFD group compared to the ND group (Fig. 3B). In the case of Ruminococcaceae and Lachnospiraceae to which butyrate-producing bacteria belong in the family level (Baxter et al., 2019). There was significant reduction in HFD-fed mice (Fig. 3C). These results showed that butyrate-producing bacteria were reduced in HFD-fed mice compared to ND-fed mice. Furthermore, the concentration of NaB in mice plasma by using gas chromatography-mass spectrometry (GC-MS) was measured to determine if the concentration of NaB in the plasma of HFD-fed mice was consistently reduced. The concentration of NaB in the plasma of HFD-fed mice was lower than in that of ND-fed mice (Fig. 4).

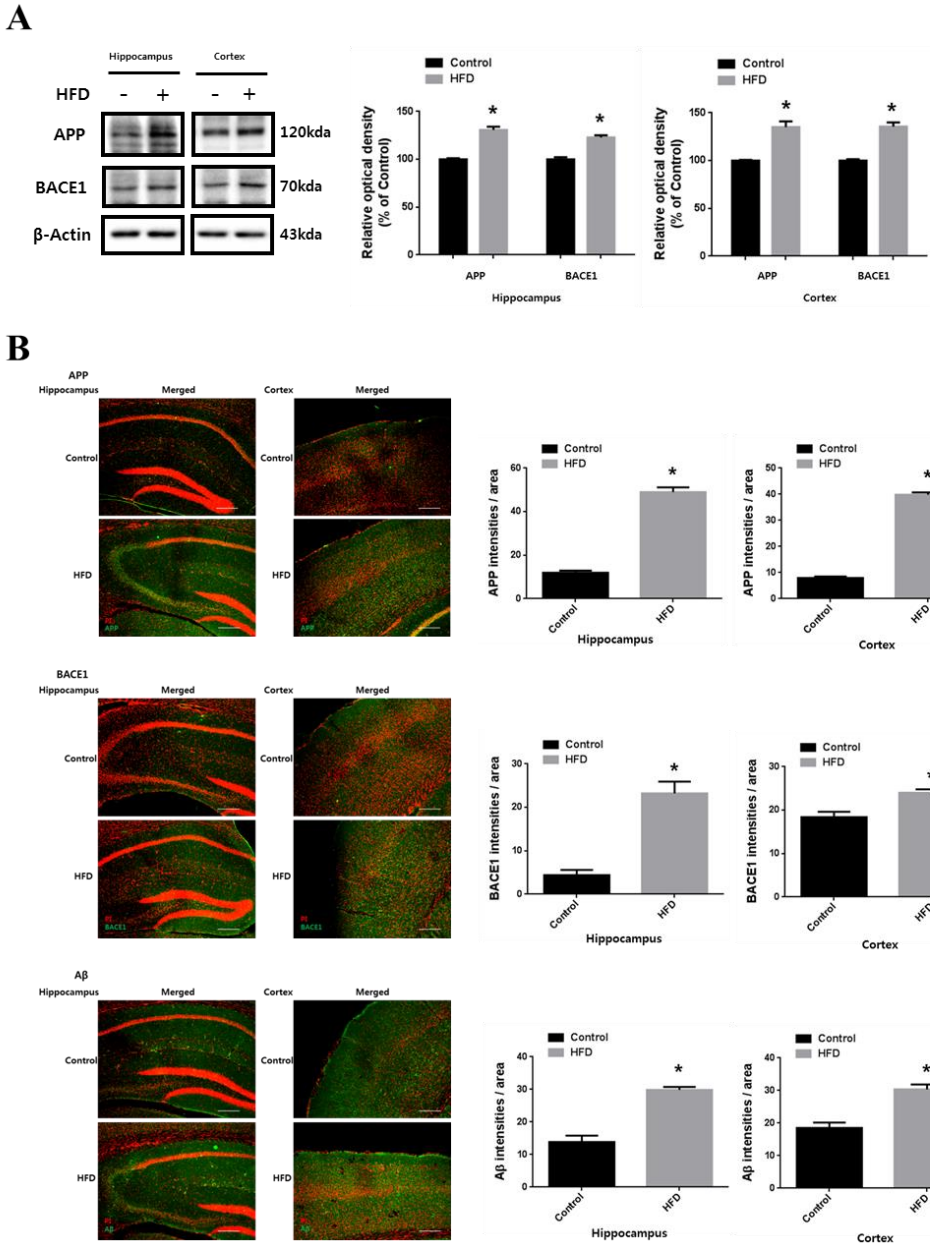
A
Hippocampus
Cortex
HFD - + - +
APP
BACE1
β-Actin
120kda
70kda
43kda
Control
HFD
Relative optical density (% of Control)
APP
BACE1
Hippocampus
Cortex
B
APP
BACE1
Aβ
Hippocampus
Cortex
Merged
Control
HFD
APP intensities / area
BACE1 intensities / area
Aβ intensities / area

Figure 1. BACE1 expression and Aβ accumulation in a brain of obesity model. (A) Brains of 20weeks old ICR mice which were fed with HFD for 14weeks were extracted. The extracted brains were cryo-sectioned coronally, and separated into hippocampus and cortex. The expression levels of APP, BACE1, and β-actin were analyzed by western blot. β-Actin was used as a loading control. Data are presented as a mean ± S.E.M. n = 4 (B) Brain samples for immunohistochemistry were immunostained with APP, BACE1, and Aβ antibodies and PI. The blot and immunofluorescence images shown are representative. All scale bars, 25μm (magnification, × 100).

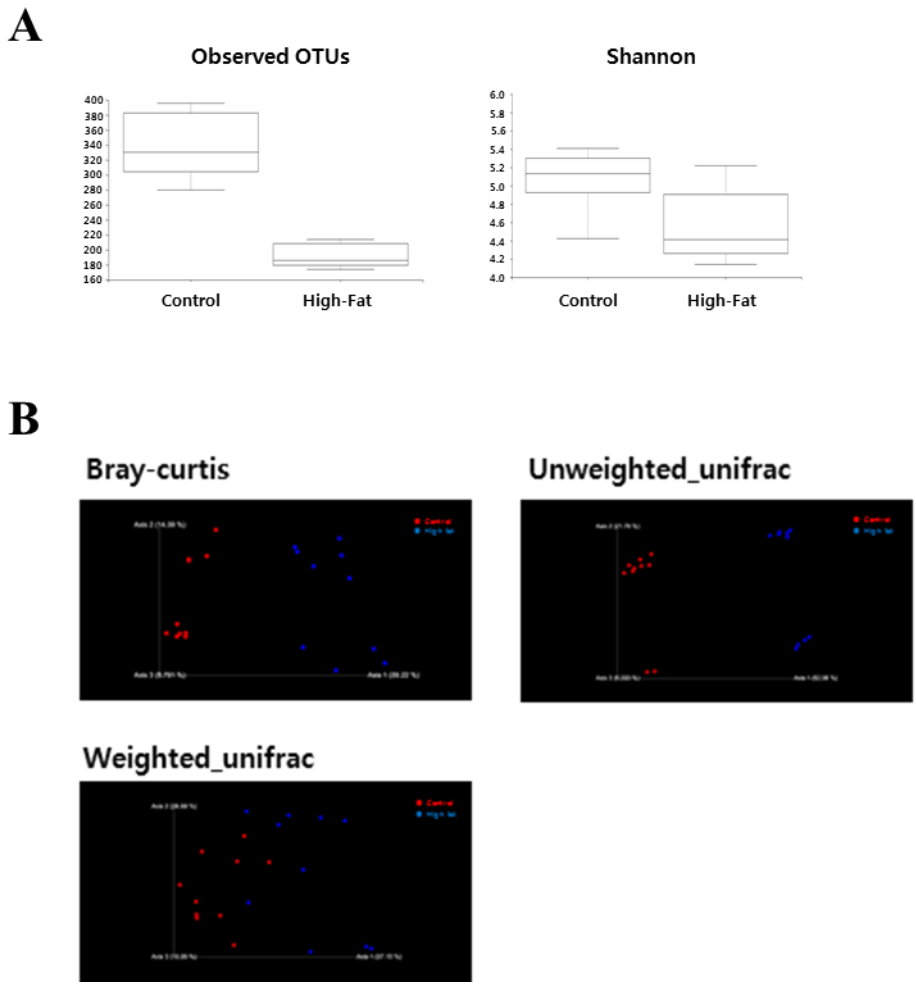

Figure 2. Effect of obesity on the gut microbiota diversity in mice model. (A) Alpha diversity between control and high-fat; left panel: Observed OTUs, right panel: Shannon's diversity index (B) Beta diversity between control (●) and high-fat (●); Bray-Curtis, unweighted UniFrac distance, weighted UniFrac distance.

A

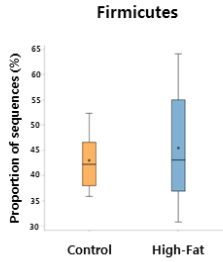

Feature	Diff. between means	p-value
p__Bacteroidetes	7.260	0.041
p__Verrucomicrobia	-6.134	0.100
p__Deferribacteres	-0.205	0.193
p__Tenericutes	-0.284	0.287
p__Proteobacteria	2.282	0.318
p__TM7	-0.022	0.343
p__Actinobacteria	-0.432	0.450
p__Firmicutes	-2.473	0.577
Unclassified k__Bacteria	0.007	0.616

B

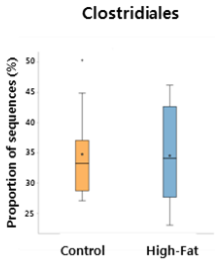

Feature	Diff. between means	p-value
o__Turicibacterales	1.576	1.05e-3
o__SHA-98	0.025	1.17e-3
o__Coriobacteriales	-0.937	2.28e-3
o__Erysipelotrichales	-1.749	8.71e-3
o__Bacteroidales	7.260	0.041
o__RF32	4.000	0.076
o__Verrucomicrobiales	-6.134	0.100
o__Bacillales	-0.083	0.141
o__Burkholderiales	-1.821	0.148
o__Deferribacterales	-0.205	0.193

o__Bifidobacteriales	0.505	0.256
o__RF39	-0.035	0.298
o__Anaeroplasmatales	-0.249	0.309
o__I025	-0.022	0.343
o__Lactobacillales	-2.467	0.379
Unclassified k__Bacteria	0.007	0.616
o__Enterobacteriales	0.103	0.776
o__Clostridiales	0.226	0.951

C

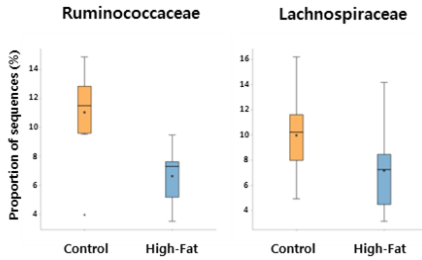

Feature	Diff. between means	p-value
f__Peptococcaceae	-2.063	7.45e-5
f__Peptostreptococcaceae	-2.939	2.71e-4
f__Turicibacteraceae	1.576	1.05e-3
Unclassified o__SHA-98	0.025	1.17e-3
f__Ruminococcaceae	4.398	1.84e-3
f__Coriobacteriaceae	-0.937	2.28e-3
f__S24-7	2.525	3.74e-3
f__Streptococcaceae	-0.122	4.85e-3
f__Erysipelotrichaceae	-1.749	8.71e-3
f__Porphyromonadaceae	-3.452	9.10e-3
f__Bacteroidaceae	8.187	0.011
f__Clostridiaceae	-0.703	0.040
f__Enterococcaceae	-0.392	0.042
Unclassified o__RF32	4.000	0.076
f__Lachnospiraceae	2.799	0.094
f__Dehalobacteriaceae	-0.022	0.099
f__Verrucomicrobiaceae	-6.134	0.100
f__Christensenellaceae	-0.030	0.124
f__Staphylococcaceae	-0.083	0.141
f__Alcaligenaceae	-1.821	0.148

f__Deferribacteraceae	-0.205	0.193
f__Bifidobacteriaceae	0.505	0.256
Unclassified o__RF39	-0.035	0.298
f__Anaeroplasmataceae	-0.249	0.309
f__Rs-045	-0.022	0.343
Unclassified o__Lactobacillales	-0.016	0.343
f__Lactobacillaceae	-1.937	0.480
f__[Mogibacteriaceae]	0.059	0.544
f__Veillonellaceae	-0.047	0.579
Unclassified o__Clostridiales	-1.226	0.595
Unclassified k__Bacteria	0.007	0.616
f__Enterobacteriaceae	0.103	0.776

Figure 3. Effect of obesity on the butyrate-producing bacteria. (A)-(C) STAMP analysis; (A) Differences in relative abundance of firmicutes between groups at the phylum level, (B) Differences in relative abundance of clostridiales between groups at the order level, (C) Differences in relative abundance of ruminococcaceae and lachnospiraceae between groups at the family level.

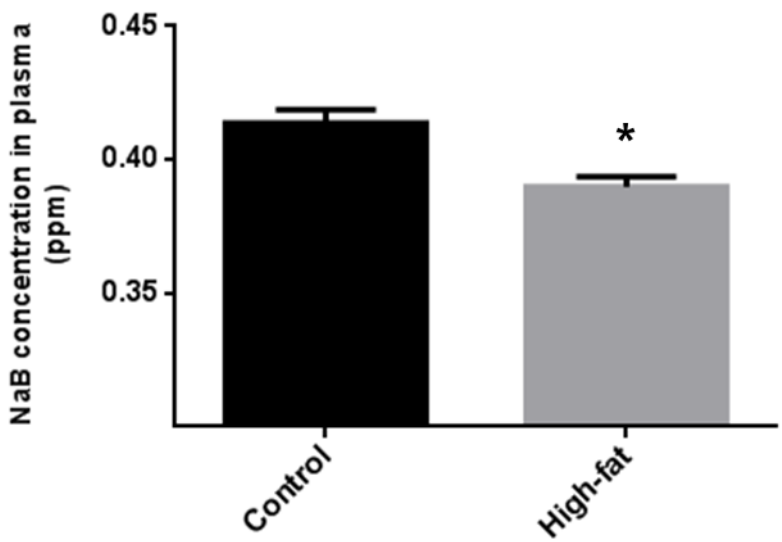

Figure 4. The concentration of NaB in the plasma of obesity model.

The concentration of NaB in plasma of mice was measured by GC-MS. NaB concentration data are presented as a mean ± S.E.M. n = 4. $^{*}p < 0.05$ versus control.

2. NaB inhibits high cholesterol-induced BACE1 expression and Aβ accumulation

To confirm the effect of high cholesterol on Aβ, this study analyzed the protein expression levels of APP and BACE1 in SK-N-MC cells treated with high cholesterol for 0 to 48h. High cholesterol significantly increased the expression levels of APP and BACE1 at 24 to 48h (Fig. 5). It was investigated whether NaB affects the expression levels of APP, BACE1, and presenilin-1 (PSEN1). My data showed that NaB decreased only high cholesterol-induced BACE1, whereas APP and PSEN1 did not show a significant change in the expression levels (Fig. 6A-B). In the immunofluorescence staining results, the fluorescence intensities of BACE1 under high cholesterol conditions were increased, but those of BACE1 were decreased by NaB (Fig. 6C). In these results, when Aβ concentration levels were measured in medium samples by enzyme-linked immunosorbent assay (ELISA) kit, the levels in the medium treated with NaB under high cholesterol conditions were decreased (Fig. 6D). These results indicated that Aβ accumulation induced by high cholesterol was dependent on BACE1, and NaB decreased the expression levels of BACE1 and eventually blocked Aβ accumulation. Next, this study compared the effects of SCFAs,

the main metabolites of the gut microbiota, on high cholesterol-induced ROS and Aβ regulating enzymes. As shown in Fig. 7A-B, sodium propionate (NaP) and sodium acetate (NaA) did not significantly affect the expression levels of these proteins, but NaB influenced the expression levels of BACE1 (Fig. 7A). Also, NaB decreased the ROS produced by high cholesterol most (Fig. 7B). Taken together, these data suggested that the effect of NaB on the reduction of high cholesterol-induced BACE1 and Aβ is the greatest of SCFAs in SK-N-MC cells.

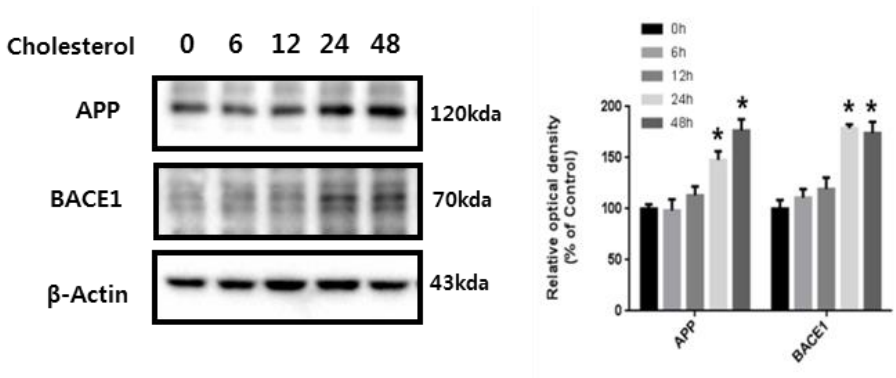

Figure 5. Effect of high cholesterol on APP and BACE1 expression in SK-N-MC cells. SK-N-MC cells were treated with high cholesterol (25 μM) for various time (0-48h). APP and BACE1 were analyzed by western blot. β-Actin was used as a loading control. Data are presented as a mean ± S.E.M. n = 4. The blot image shown is representative.

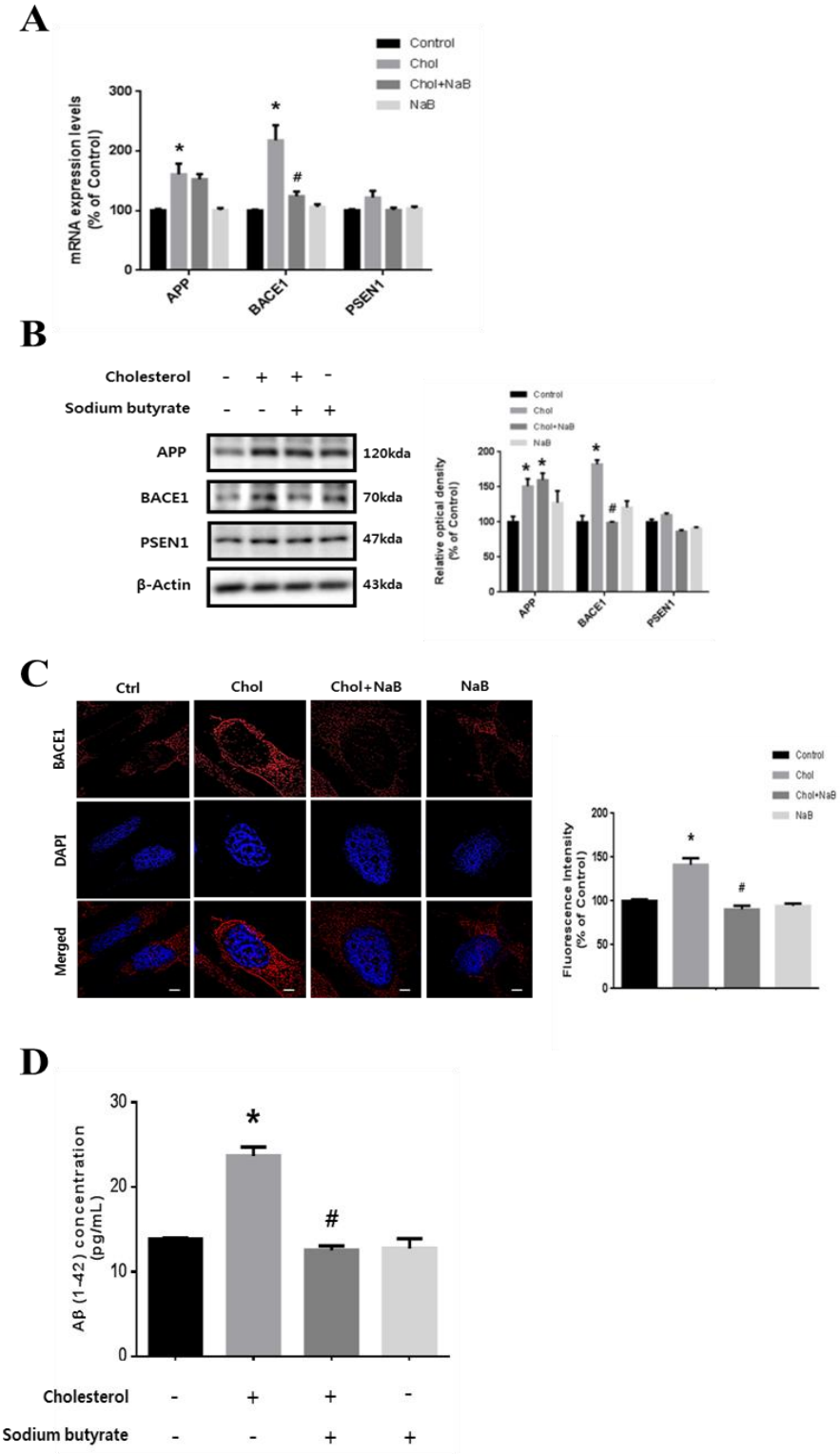
A
Control
Chol
Chol+NaB
NaB
mRNA expression levels (% of Control)
300
200
100
0
*
*
#
APP
BACE1
PSEN1
B
Cholesterol - + + -
Sodium butyrate - - + +
APP
BACE1
PSEN1
β-Actin
120kda
70kda
47kda
43kda
Relative optical density (% of Control)
200
150
100
50
0
C
Ctrl
Chol
Chol+NaB
NaB
BACE1
DAPI
Merged
Fluorescence Intensity (% of Control)
D
Aβ (1-42) concentration (pg/mL)
30
20
10
0
Cholesterol - + + -
Sodium butyrate - - + +

Figure 6. Effect of NaB on high cholesterol-induced Aβ regulating enzymes and Aβ accumulation. (A) SK-N-MC cells were pre-treated with NaB (500μM) for 30min prior to treatment of high cholesterol for 24h. mRNA expressions of APP, BACE1, and PSEN1 were analyzed by quantitative real time PCR. Data were normalized by the ACTB mRNA expression level. Data are presented as a mean ± S.E.M. n = 4. (B) Cells were pre-treated with NaB for 30min prior to treatment of high cholesterol for 24h. The expression levels of APP, BACE1, and PSEN1 were analyzed by western blot. β-Actin was used as a loading control. Data are presented as a mean ± S.E.M. n = 4. (C) Cells were pre-treated with NaB for 30min prior to treatment of high cholesterol for 24h and immunostained with BACE1 antibody. Scale bars are 8μm (magnification, × 1,000). n = 3. (D) Cells were pre-treated with NaB for 30min prior to treatment for high cholesterol for 72h. Aβ concentration of medium samples was detected by using ELISA kit. Data are presented as a mean ± S.E.M. n = 4. $^{*}p < 0.05$ versus control, $^{\#}p < 0.05$ versus high cholesterol treatment. The blot and immunofluorescence images shown are representative.

A

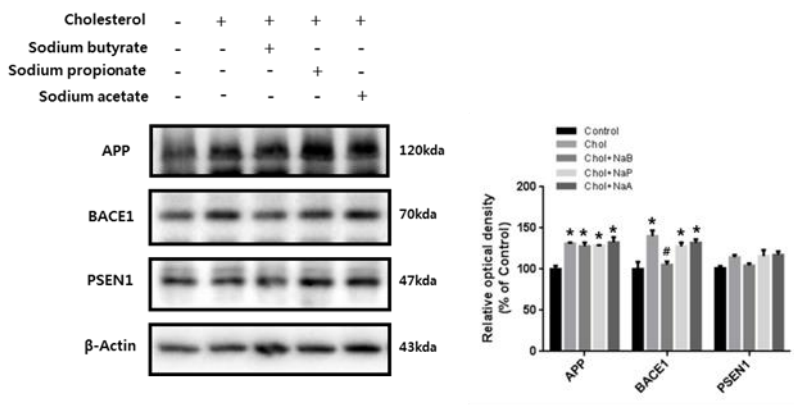
Cholesterol - + + + +
Sodium butyrate - - + - -
Sodium propionate - - - + -
Sodium acetate - - - - +
APP
120kda
BACE1
70kda
PSEN1
47kda
β-Actin
43kda
Control
Chol
Chol+NaB
Chol+NaP
Chol+NaA
Relative optical density (% of Control)
APP
BACE1
PSEN1

B

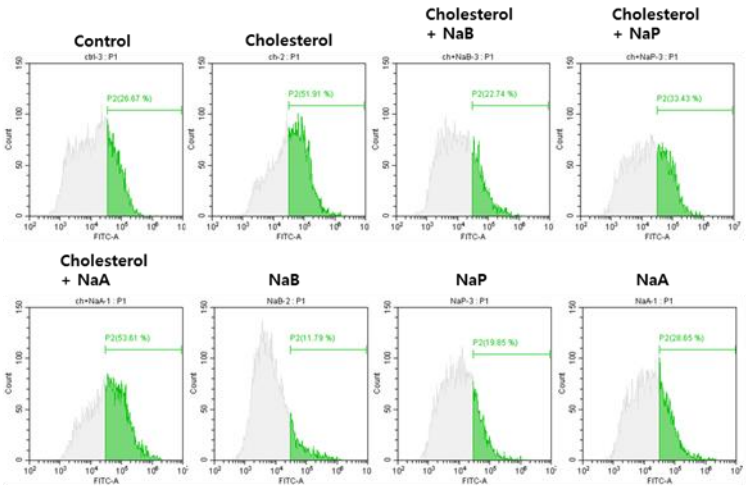
Control
Cholesterol
Cholesterol + NaB
Cholesterol + NaP
Cholesterol + NaA
NaB
NaP
NaA
FITC-A
Count

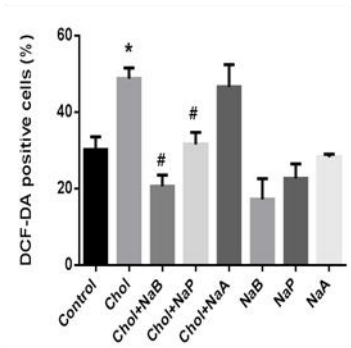
DCF-DA positive cells (%)
Control
Chol
Chol+NaB
Chol+NaP
Chol+NaA
NaB
NaP
NaA

Figure 7. Comparison of effect of SCFAs on high cholesterol-induced ROS and Aβ regulating enzymes. (A) SK-N-MC cells were pre-treated with NaB, NaP, and NaA (500μM) for 30min prior to treatment of high cholesterol for 24h. The expression levels of APP, BACE1, and PSEN1 were analyzed by western blot. β-Actin was used as a loading control. Data are presented as a mean ± S.E.M. n = 3. (B) Cells were pre-treated with NaB or NaP or NaA for 30min prior to high cholesterol treatment for 72h where ROS with DCF-DA were measured by flowcytometer. Total cell counts = 1.0×10^4 cells. Data are presented as a mean ± S.E.M. n = 4. $^{*}p < 0.05$ versus control, $^{\#}p < 0.05$ versus high cholesterol treatment. The blot image shown is representative.

3. NaB inhibits high cholesterol-induced NOX2 expression

To determine the main site of excessive ROS produced by high cholesterol in SK-N-MC cells, we pretreated Vas2870 (NOX inhibitor) and mitotempo (inhibitor of mtROS generation) under high cholesterol conditions. High cholesterol-induced ROS were blocked by Vas2870 but not by mitotempo (Fig. 8A). This study also checked by staining with MitoSOX^{TM} Red to confirm that mtROS is critically produced by high cholesterol. In the results, mtROS produced by high cholesterol did not show a significant increase (Fig. 8B). Previous studies reported that the most prominent transcription factor of NOX2 is nuclear factor-kappa B (NF-κB) (Manea et al., 2015). The results showed that NF-κB levels were increased by high cholesterol in the nucleus, but decreased by NaB (Fig. 9A). Consistently, immunofluorescence illustrated that a number of NF-κB accumulated around the nucleus, but scattered to the cytoplasm by NaB under high cholesterol conditions (Fig. 9B). This study further investigated whether NF-κB is a critical transcription factor for NOX2 in SK-N-MC cells. The increased expression levels of NOX2 under high cholesterol conditions were decreased by Bay11-7082 (NF-κB inhibitor) (Fig. 9C). Previous

studies reported that NOX1-4 are major isotypes of NOX expressed in the brain, and there seems to be a difference in expression depending on cell types (Cooney et al., 2013; Hernandes et al., 2012). Therefore, primers referring to the previous studies were made and gradient PCR was performed with complementary DNA of SK-N-MC cells (Auer et al., 2017; De la Monte et al., 2006). The results showed that NOX1 and NOX3 were hardly expressed in SK-N-MC cells (Fig. 10A), and thereby real-time PCR was performed with NOX2 and NOX4 as major isotypes. In the results, the mRNA expression levels of NOX2 showed the greater increase in SK-N-MC cells exposed to high cholesterol and significantly decreased by NaB (Fig. 10B). Consistently, the protein expression levels of NOX2 were also significantly increased by high cholesterol and decreased by NaB (Fig. 10C). Collectively, these results suggested that increased NOX2 by high cholesterol is a major cause of overproduced ROS, and NaB disturbs the nuclear translocation of NF-κB, eventually reducing NOX2 expression and inhibiting overproduced ROS. The increased expression levels of BACE1 by high cholesterol were significantly decreased by treating N-acetylcysteine (NAC; ROS scavenger) and Vas2870, but not mitotempo (Fig. 11A). Consistently, Aβ concentration levels in the medium treated with NAC and Vas2870 under high cholesterol conditions were decreased, but not in the medium treated with mitotempo (Fig. 11B).

A

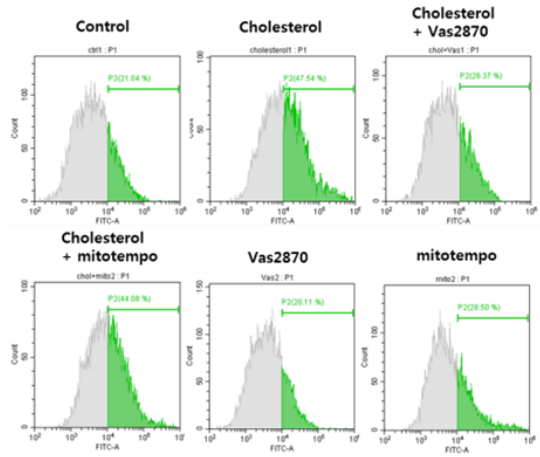
Control
Cholesterol
Cholesterol + Vas2870
Cholesterol + mitotempo
Vas2870
mitotempo
FITC-A
Count

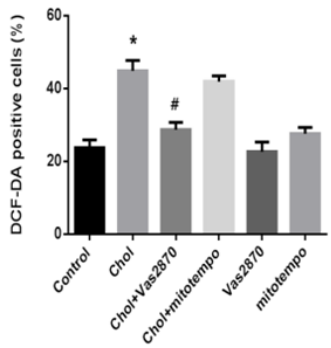
DCF-DA positive cells (%)
Control
Chol
Chol+Vas2870
Chol+mitotempo
Vas2870
mitotempo

B

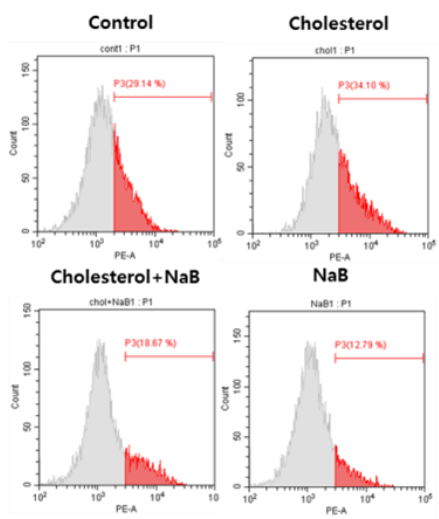
Control
Cholesterol
Cholesterol+NaB
NaB
PE-A
Count

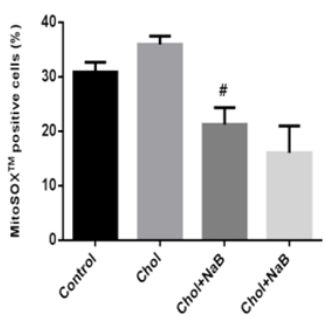
MitoSOX™ positive cells (%)
Control
Chol
Chol+NaB
Chol+NaB

Figure 8. Involvement of NOX in high cholesterol-induced ROS. (A) SK-N-MC cells were pre-treated with either Vas2870 (5 μM) or mitotempo (2 μM) for 30min prior to high cholesterol treatment for 72h where ROS with DCF-DA were measured by flowcytometer. Total cell counts = 1.0×10^4 cells. Data are presented as a mean ± S.E.M. n = 4. $^{*}p < 0.05$ versus control, $^{\#}p < 0.05$ versus high cholesterol treatment. (B) Cells were pre-treated with NaB for 30min prior to high cholesterol treatment for 72h where mtROS with MitoSOX^{TM} red were measured by flowcytometer. Total cell counts = 1.0×10^4 cells. Data are presented as a mean ± S.E.M. n = 4. $^{\#}p < 0.05$ versus high cholesterol treatment.

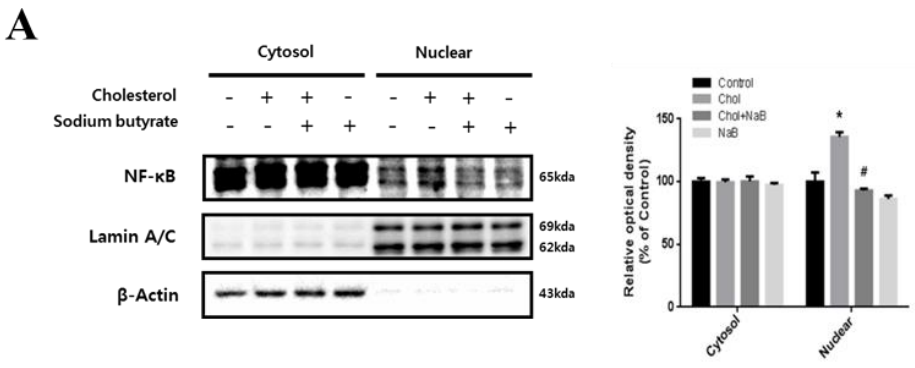
A
Cytosol
Nuclear
Cholesterol
Sodium butyrate
NF-κB
Lamin A/C
β-Actin
65kda
69kda
62kda
43kda
Control
Chol
Chol+NaB
NaB
Relative optical density (% of Control)
Cytosol
Nuclear

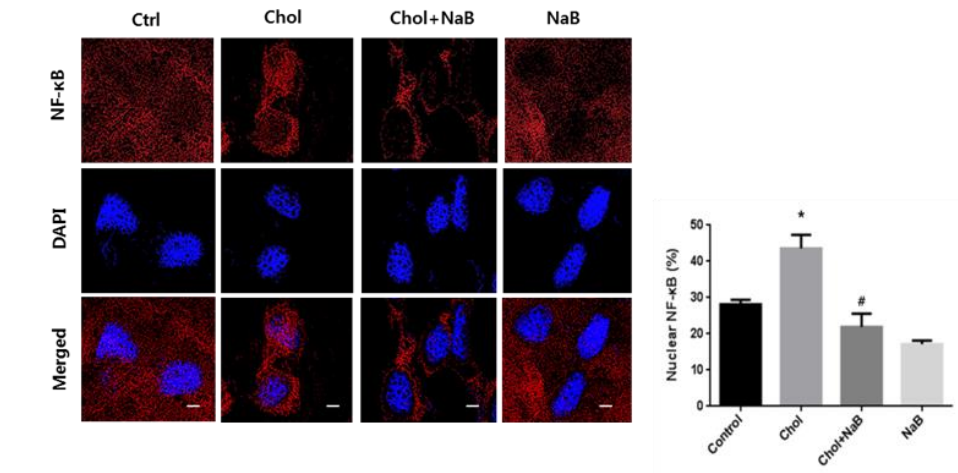
B
Ctrl
Chol
Chol+NaB
NaB
NF-κB
DAPI
Merged
Nuclear NF-κB (%)
Control
Chol
Chol+NaB
NaB

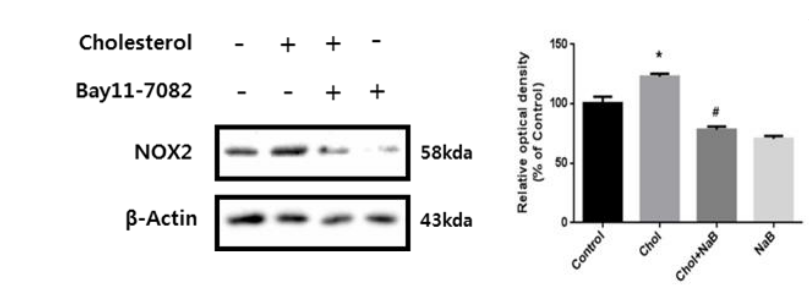
C
Cholesterol
Bay11-7082
NOX2
β-Actin
58kda
43kda
Relative optical density (% of Control)
Control
Chol
Chol+NaB
NaB

Figure 9. Involvement of NF-κB in high cholesterol-induced NOX2.

(A) SK-N-MC cells were pre-treated with NaB for 30min prior to high cholesterol treatment for 24h. NF-κB, lamin A/C, and β-actin protein levels in cytosolic and nuclear fractionized samples were analyzed by western blot. Data are presented as a mean ± S.E.M. n = 3. $^{*}p < 0.05$ versus control, $^{\#}p < 0.05$ versus high cholesterol treatment. (B) Cells were pre-treated with NaB for 30min prior to high cholesterol treatment for 24h and immunostained with NF-κB antibody. Scale bars are 8μm (magnification, × 1,000). n = 3. $^{*}p < 0.05$ versus control, $^{\#}p < 0.05$ versus high cholesterol treatment. (C) Cells were pre-treated with Bay11-7082 (5μM) for 30min prior to high cholesterol treatment for 24h. The expression levels of NOX2 were analyzed by western blot. β-Actin was used as a loading control. Data are presented as a mean ± S.E.M. n = 3. $^{*}p < 0.05$ versus control, $^{\#}p < 0.05$ versus high cholesterol treatment. All blot and immunofluorescence images shown are representative.

A

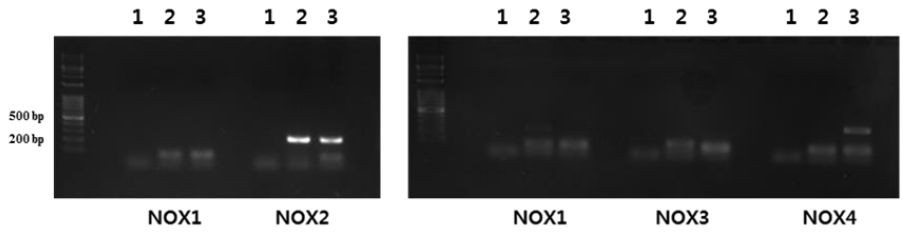
1 2 3 1 2 3
1 2 3 1 2 3 1 2 3
500 bp
200 bp
NOX1 NOX2
NOX1 NOX3 NOX4

B

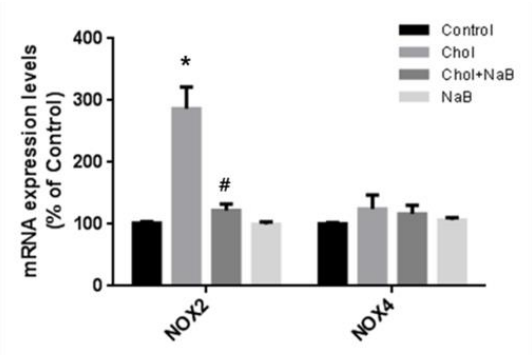
mRNA expression levels (% of Control)
400
300
200
100
0
*
#
Control
Chol
Chol+NaB
NaB
NOX2
NOX4

C

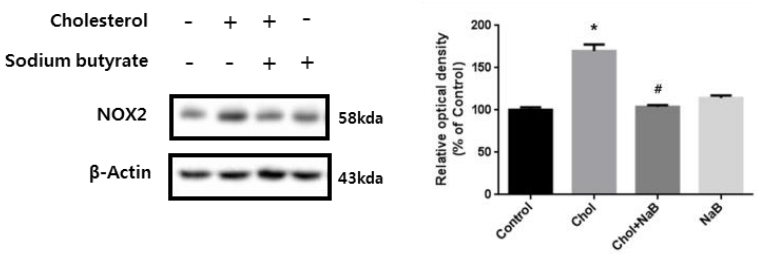
Cholesterol - + + -
Sodium butyrate - - + +
NOX2
58kda
β-Actin
43kda
Relative optical density (% of Control)
200
150
100
50
0
*
#
Control
Chol
Chol+NaB
NaB

Figure 10. Effect of NaB on high cholesterol-induced NOX2. (A) SK-N-MC cells were pre-treated with NaB for 30min prior to high cholesterol treatment for 24h. Gradient PCR was performed with complementary DNA of SK-N-MC cells. 1: 52℃, 2: 55℃, 3: 58℃. Optimum annealing temperature was set at 58℃. (B) Cells were pre-treated with NaB for 30min prior to high cholesterol treatment for 24h. Data were normalized by the ACTB mRNA expression level. Data are presented as a mean ± S.E.M. n = 4. $^{*}p < 0.05$ versus control, $^{\#}p < 0.05$ versus high cholesterol treatment. (C) Cells were pre-treated with NaB for 30min prior to high cholesterol treatment for 24h. The expression levels of NOX2 were analyzed by western blot. β-Actin was used as a loading control. Data are presented as a mean ± S.E.M. n = 4. $^{*}p < 0.05$ versus control, $^{\#}p < 0.05$ versus high cholesterol treatment. All blot images shown are representative.

A

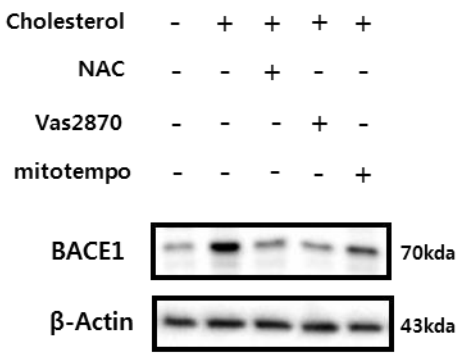
Cholesterol - + + + +
NAC - - + - -
Vas2870 - - - + -
mitotempo - - - - +
BACE1
70kda
β-Actin
43kda

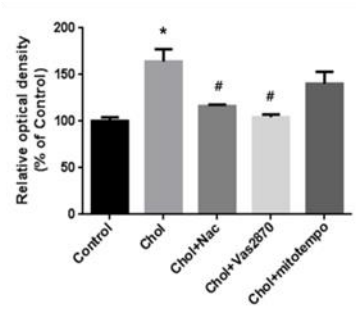
Relative optical density (% of Control)
200
150
100
50
0
*
#
#
Control
Chol
Chol+Nac
Chol+Vas2870
Chol+mitotempo

B

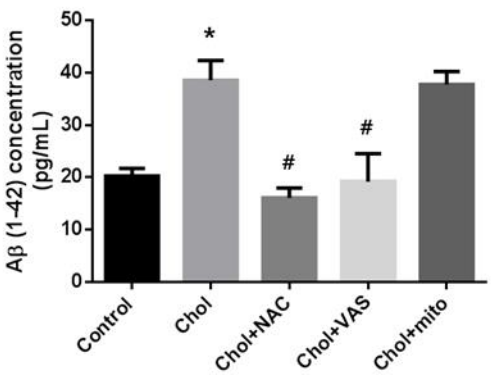
Aβ (1-42) concentration (pg/mL)
50
40
30
20
10
0
*
#
#
Control
Chol
Chol+NAC
Chol+VAS
Chol+mito

Figure 11. Effect of ROS produced by NOX2 under high cholesterol on BACE1 and Aβ. (A) SK-N-MC cells were pre-treated with either NAC (5mM), Vas2870 (5 μM) or mitotempo (2 μM) for 30min prior to high cholesterol treatment for 48h. The expression levels of BACE1 were analyzed by western blot. β-Actin was used as a loading control. Data are presented as a mean ± S.E.M. n = 3. $^{*}p < 0.05$ versus control, $^{\#}p < 0.05$ versus high cholesterol treatment. (B) Cells were pre-treated with either NAC (5mM), Vas2870 (5 μM) or mitotempo (2 μM) for 30min prior to high cholesterol treatment for 72h. Aβ concentration of medium samples was detected by using ELISA kit. Data are presented as a mean ± S.E.M. n = 4. $^{*}p < 0.05$ versus control, $^{\#}p < 0.05$ versus high cholesterol treatment. The blot image shown is representative.

4. Regulatory role of NaB in high cholesterol-induced downregulation of p21 and p21/Nrf2 co-localization

The study investigated the effect of NaB on the nuclear translocation of Nrf2 in SK-N-MC cells under high cholesterol conditions. The levels of Nrf2 in the nucleus were decreased by high cholesterol, but were increased by NaB (Fig. 12A). Consistently, immunofluorescence showed that a number of Nrf2 accumulated in the cytoplasm under high cholesterol conditions, but accumulated around the nucleus by NaB (Fig. 12B). In the results, either p53 or sp1, which are the most prominent transcription factors of p21 (Koutsodontis et al., 2001), sp1 was decreased in migration to the nucleus under high cholesterol conditions, but increased by NaB, whereas the nuclear translocation of p53 was increased under high cholesterol conditions, but decreased by NaB (Fig. 13A-C). NaB is a representative HDAC inhibitor. Previous study has shown that the acetylation of transcription factors affects the nuclear translocation (Kundumani-Sridharan et al., 2012). Therefore, this study verified whether the acetylation of sp1 facilitates the nuclear translocation of sp1. Pretreatment of ibuprofen with NaB under high cholesterol conditions resulted in a decrease of sp1 migration to the nucleus (Fig. 14A). This study

also confirmed the increase of nuclear translocation through sp1 acetylation by pretreating C646 (p300/CBP inhibitor) which inhibits sp1 acetylation. In the results, the nuclear translocation of sp1 was decreased after pretreating with C646 with NaB under high cholesterol conditions (Fig. 14B). This study determined whether the expression levels of p21 are increased by NaB under high cholesterol conditions. The data showed that the expression levels of p21 were decreased by high cholesterol compared to control levels, but were recovered by NaB (Fig. 15A). The study confirmed that the co-localization of p21 and Nrf2 was decreased by high cholesterol, but increased by NaB (Fig. 15B). However, since p21 is an apoptosis marker or apoptosis inhibition marker, it was verified whether NaB induces apoptosis or not. The cell viability was decreased by high cholesterol, but recovered by NaB (Fig. 15C-D).

A

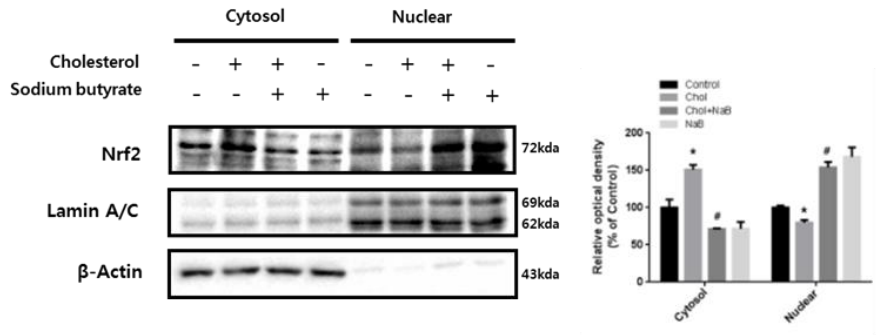
Cytosol
Nuclear
Cholesterol
Sodium butyrate
Nrf2
Lamin A/C
β-Actin
72kda
69kda
62kda
43kda
Control
Chol
Chol+NaB
NaB
Relative optical density (% of Control)
Cytosol
Nuclear

B

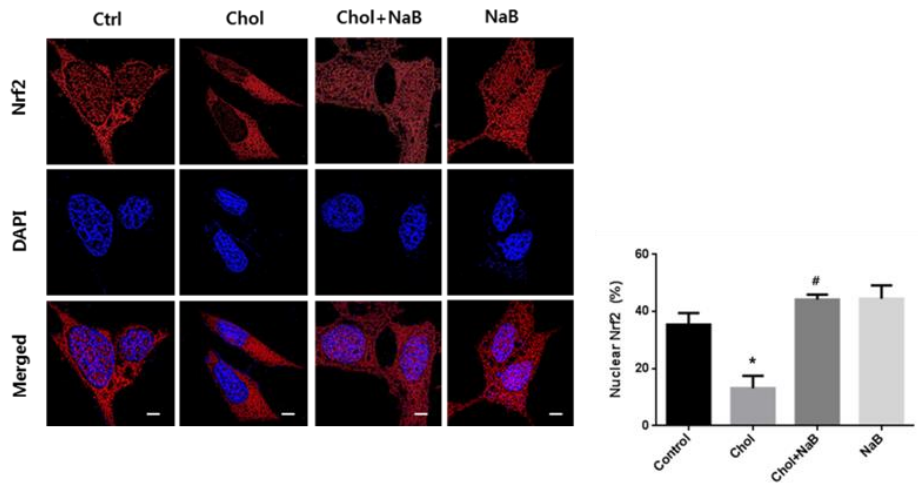
Ctrl
Chol
Chol+NaB
NaB
Nrf2
DAPI
Merged
Nuclear Nrf2 (%)
Control
Chol
Chol+NaB
NaB

Figure 12. Effect of NaB on the nuclear translocation of Nrf2. (A) SK-N-MC cells were pre-treated with NaB for 30min prior to high cholesterol treatment for 24h. Nrf2, lamin A/C, and β-actin protein levels in cytosolic and nuclear fractionized samples were analyzed by western blot. Data are presented as a mean ± S.E.M. n = 3. $^{*}p < 0.05$ versus control, $^{\#}p < 0.05$ versus high cholesterol treatment. (B) Cells were immunostained with Nrf2 antibody. Scale bars are 8μm (magnification, × 1,000). n = 3. $^{*}p < 0.05$ versus control, $^{\#}p < 0.05$ versus high cholesterol treatment. All blot and immunofluorescence images shown are representative.

A

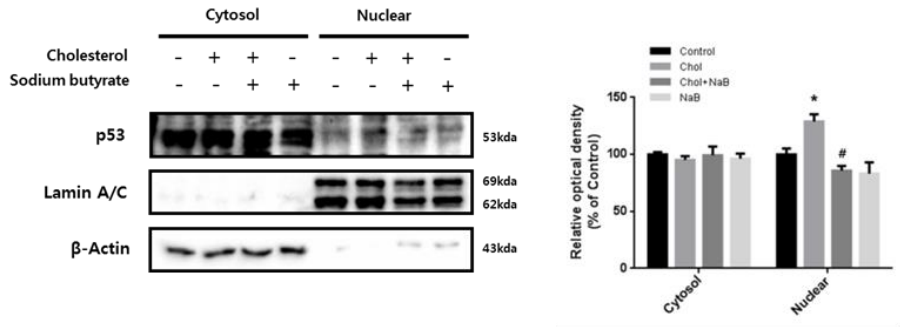
Cytosol
Nuclear
Cholesterol
Sodium butyrate
p53
Lamin A/C
β-Actin
53kda
69kda
62kda
43kda
Control
Chol
Chol+NaB
NaB
Relative optical density (% of Control)
Cytosol
Nuclear

B

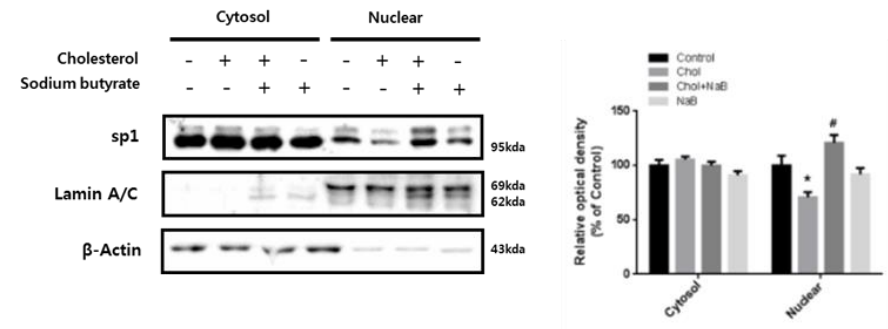
Cytosol
Nuclear
Cholesterol
Sodium butyrate
sp1
Lamin A/C
β-Actin
95kda
69kda
62kda
43kda
Control
Chol
Chol+NaB
NaB
Relative optical density (% of Control)
Cytosol
Nuclear

C

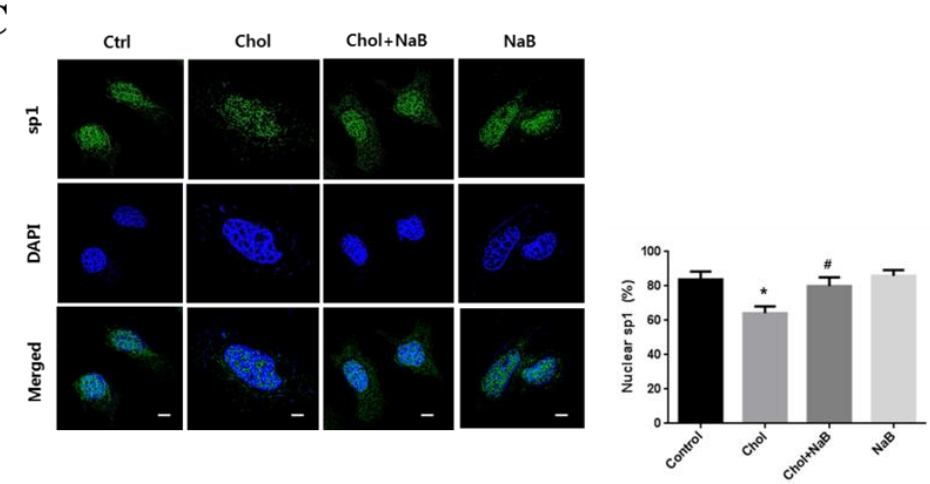
Ctrl
Chol
Chol+NaB
NaB
sp1
DAPI
Merged
Nuclear sp1 (%)
Control
Chol
Chol+NaB
NaB

Figure 13. Effect of NaB on the nuclear translocation of p53 and sp1.

(A) SK-N-MC cells were pre-treated with NaB for 30min prior to high cholesterol treatment for 24h. p53, lamin A/C, and β-actin protein levels in cytosolic and nuclear fractionized samples were analyzed by western blot. Data are presented as a mean ± S.E.M. n = 3. $^{*}p < 0.05$ versus control. (B) Cells were pre-treated with NaB for 30min prior to high cholesterol treatment for 24h. Sp1, lamin A/C, and β-actin protein levels in cytosolic and nuclear fractionized samples were analyzed by western blot. Data are presented as a mean ± S.E.M. n = 3. $^{*}p < 0.05$ versus control, $^{\#}p < 0.05$ versus high cholesterol treatment. (C) Cells were immunostained with sp1 antibody. Scale bars are 8μm (magnification, × 1,000). n = 5. $^{*}p < 0.05$ versus control, $^{\#}p < 0.05$ versus high cholesterol treatment. All blot and immunofluorescence images shown are representative.

A

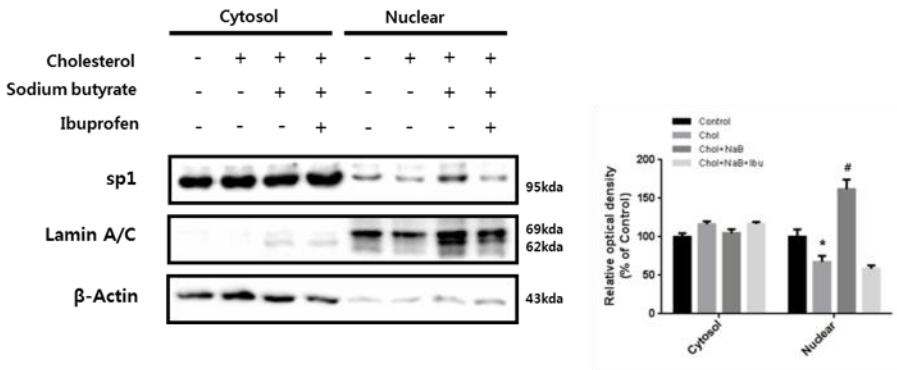
Cytosol
Nuclear
Cholesterol
Sodium butyrate
Ibuprofen
sp1
Lamin A/C
β-Actin
95kda
69kda
62kda
43kda
Control
Chol
Chol+NaB
Chol+NaB+Ibu
Relative optical density (% of Control)
Cytosol
Nuclear

B

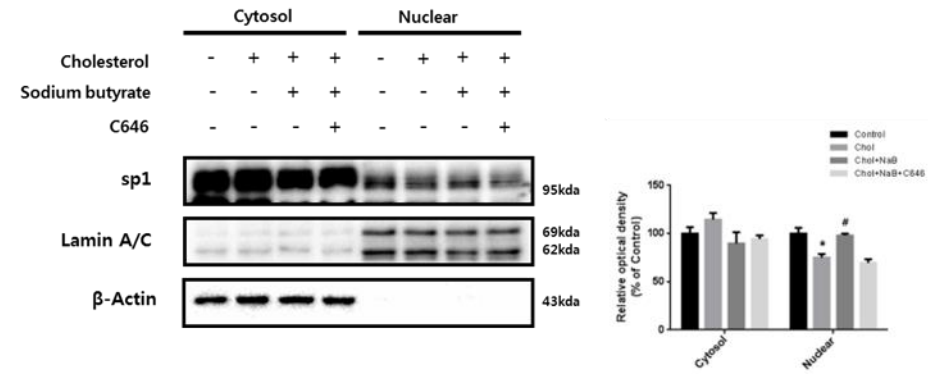
Cytosol
Nuclear
Cholesterol
Sodium butyrate
C646
sp1
Lamin A/C
β-Actin
95kda
69kda
62kda
43kda
Control
Chol
Chol+NaB
Chol+NaB+C646
Relative optical density (% of Control)
Cytosol
Nuclear

Figure 14. Effect of sp1 acetylation on the nuclear translocation of sp1. (A) SK-N-MC cells were pre-treated with NaB and ibuprofen for 30min prior to treatment of high cholesterol for 24h. Sp1, lamin A/C, and β-actin protein levels in cytosolic and nuclear fractionized samples were analyzed by western blot. Data are presented as a mean ± S.E.M. n = 3. $^{*}p < 0.05$ versus control, $^{\#}p < 0.05$ versus high cholesterol treatment, $^{\$}p < 0.05$ versus treatment of high cholesterol and NaB. (B) Cells were pre-treated with NaB and pertussis toxin for 30min prior to treatment of high cholesterol for 24h. Sp1, lamin A/C, and β-actin protein levels in cytosolic and nuclear fractionized samples were analyzed by western blot. Data are presented as a mean ± S.E.M. n = 3. $^{*}p < 0.05$ versus control, $^{\#}p < 0.05$ versus high cholesterol treatment. All blot images shown are representative.

A

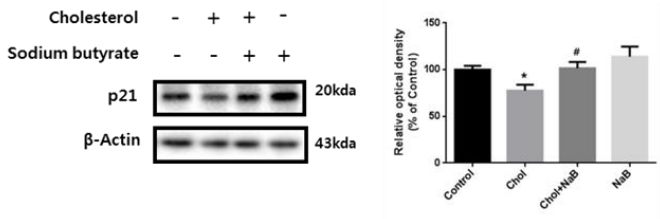
Cholesterol - + + -
Sodium butyrate - - + +
p21
β-Actin
20kda
43kda
Relative optical density (% of Control)
150
100
50
0
*
#
Control
Chol
Chol+NaB
NaB

B

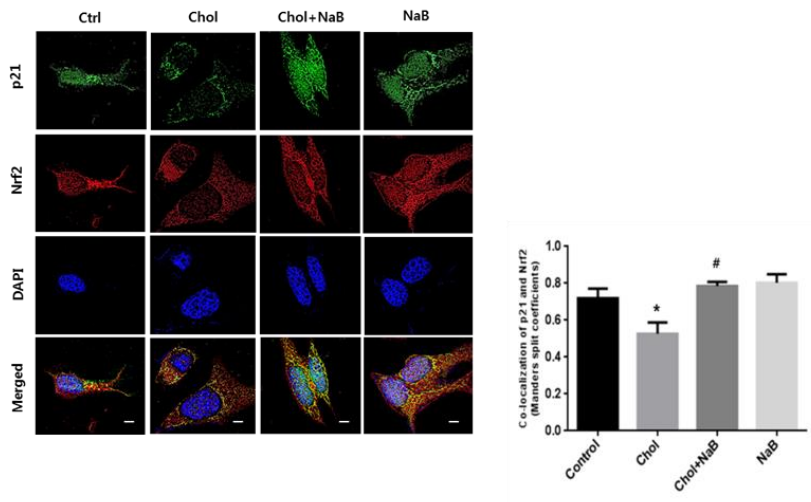
Ctrl
Chol
Chol+NaB
NaB
p21
Nrf2
DAPI
Merged
Co-localization of p21 and Nrf2 (Manders split coefficients)
1.0
0.8
0.6
0.4
0.2
0.0
*
#
Control
Chol
Chol+NaB
NaB

C

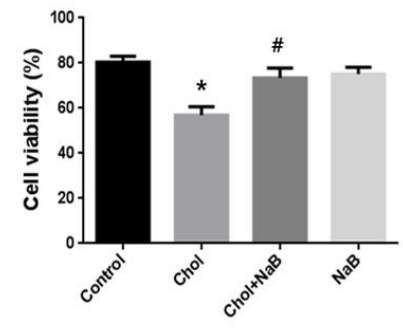
Cell viability (%)
100
80
60
40
20
0
*
#
Control
Chol
Chol+NaB
NaB

D

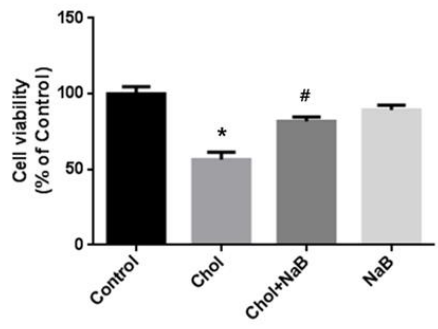
Cell viability (% of Control)
150
100
50
0
*
#
Control
Chol
Chol+NaB
NaB

Figure 15. Effect of NaB on p21 expression, p21/Nrf2 co-localization, and cell viability. (A) SK-N-MC cells were pre-treated with NaB for 30min prior to high cholesterol treatment for 24h. The expression levels of p21 were analyzed by western blot. β-Actin was used as a loading control. Data are presented as a mean ± S.E.M. n = 4. $^{*}p < 0.05$ versus control, $^{\#}p < 0.05$ versus high cholesterol treatment. (B) Cells were pre-treated with NaB for 30min prior to high cholesterol treatment for 24h and immunostained with p21 and Nrf2 antibodies. Co-localization of p21 (green) and Nrf2 (red) was visualized with SRRF imaging system. Scale bars are 8 μm (magnification, × 1,000). n = 4. $^{*}p < 0.05$ versus control, $^{\#}p < 0.05$ versus high cholesterol treatment. All blot and immunofluorescence images shown are representative. (C) Cells were pre-treated with NaB for 30min prior to high cholesterol treatment for 48h. Trypan blue stained or unstained cells were counted by using the Countess. Data are presented as a mean ± S.E.M. n = 4. $^{*}p < 0.05$ versus control, $^{\#}p < 0.05$ versus high cholesterol treatment. (D) Cells were pre-treated with NaB for 30min prior to high cholesterol treatment for 72h. The absorbance of each sample was measured by using a microplate reader. Cell viability of SK-N-MC cells was measured by WST-1 assay. Data are presented as a mean ± S.E.M. n = 5. $^{*}p < 0.05$ versus control, $^{\#}p < 0.05$ versus high cholesterol treatment. All blot and immunofluorescence images shown are representative.

DISCUSSION

This study demonstrates the dual antioxidant effect of NaB on high cholesterol-induced excessive ROS in SK-N-MC cells, ultimately inhibiting BACE1-dependent amyloidogenesis caused by excessive ROS. Although the antioxidant effect of NaB is well known (Canani et al., 2011; Jahns et al., 2015), the regulatory role of NaB to inhibit Aβ through an antioxidant effect in neurons exposed to high cholesterol environment has not been reported. In other words, this is the first study to report the mechanisms of Aβ reduction through the dual antioxidant effect of NaB under high cholesterol conditions. This study focused on the microbiota composition in obese patients who are more likely to get AD, because butyrate-producing bacteria have been observed to decrease in the gut of obese patients. Therefore, the study investigated the butyrate-producing bacteria that generally belong to Firmicutes at the phylum level: in previous studies, the alteration of Firmicutes in the gut of obese patients or HFD-fed mice is controversial (Chakraborti. 2015; Duncan et al., 2008; Harris et al., 2012). The data showed that the Firmicutes were hardly changed in HFD-fed mice, which indicates that different results appear to be

dependent on age, sex, mouse types or strains, and breeding conditions such as type of diet and housing density, so it is necessary to conduct further investigations. Therefore, plasma from mice was collected and this study measured the concentrations of NaB to see if there was actually less NaB from obese mice. The results showed lower concentrations of NaB in obese mice plasma, which suggests the cross of NaB into the blood brain barrier can be lower in obese patients. These findings suggested that the alteration of microbiota composition that butyrate-producing bacteria were reduced by HFD can be a major cause of AD induced by obesity. Thus, NaB can be a potential therapeutic substance for AD patients caused by obesity.

Furthermore, because Aβ accumulation is generally caused by the increase of APP or Aβ-producing enzymes (BACE1 and PSEN1), their expression levels in SK-N-MC cells treated with high cholesterol and NaB were confirmed. The data revealed that NaB significantly reduced the expression levels of only BACE1, which seems to be dependent on cell or treated drug type. In this study, the inhibitory effect of SCFAs, a representative fermentation product of microbiota, on amyloidogenesis was compared. Because NaP is a representative HDAC inhibitor like NaB, and both NaA and NaP act as GPCR ligands and affect cell signaling in various ways (Lu et al., 2016; Silva et al., 2018), it is necessary to confirm

whether NaB has a stronger inhibitory effect on high cholesterol-induced Aβ production compared to other SCFAs. In these results, only NaB was found to significantly affect the reduction in the expression levels of BACE1. Therefore, this study hypothesized that NaB inhibits high cholesterol-induced Aβ accumulation through the reduction of BACE1 in SK-N-MC cells.

Excessive ROS are produced in SK-N-MC cells exposed to high cholesterol environment, and these ROS are one of the major causes of AD. A number of studies described mtROS as the major source of excessive ROS, when various cells including neuronal cells are exposed to lethal conditions such as high cholesterol or high glucose (Fakhruddin et al., 2017; Zhang et al., 2012). Recently, however, there is an increasing number of studies describing the major sources of pathological oxidative stress as NOX family in the CNS, such as microglia and astrocytes as well as neurons (Nayernia et al., 2014). Thus, the major ROS sources appear to be dependent on neuronal cell types or concentrations, times, and types of treatment drug, so further studies are needed. Therefore, this study investigated the major ROS source under high cholesterol conditions by treating Vas2870 and mitotempo, because the major ROS source of SK-N-MC cells in hypercholesterolemic environment is not known. The results showed high cholesterol-induced ROS is significantly reduced by Vas2870 but not mitotempo,

which indicates that excessive ROS of SK-N-MC cells exposed to high cholesterol environment are mainly produced by NOX. Collectively, the results indicate that the major source of excessive ROS induced by high cholesterol in SK-N-MC cells is NOX2. This study thereby demonstrated that NaB under high cholesterol conditions prevents overproduced ROS through the reduction of NOX2 expression levels. In other words, one of the antioxidant effects of NaB on neuronal cells exposed to a high cholesterol environment is to reduce NOX2 expression and thus prevent ROS production itself, which can be said that Aβ accumulation of neuronal cells under high cholesterol conditions is inhibited by NaB through reduction of expression levels of NOX2.

It has been reported that the expression levels of antioxidant enzymes are increased as a protective effect against oxidative stress, whereas oxidative damage such as hyperglycemia inhibits Nrf2 pathway, which makes cells vulnerable to oxidative stress. In the results, Nrf2 migration to the nucleus in SK-N-MC cells was reduced under high cholesterol conditions, and consistent with previous studies that NaB activates Nrf2, NaB increased the nuclear translocation of Nrf2 under high cholesterol conditions. However, the specific mechanisms of the antioxidant effect of NaB on the oxidative damage caused by high cholesterol are not known yet. Previous researchers have shown that p21 is co-localized with

Nrf2, which stabilizes Nrf2 to facilitate nuclear translocation of Nrf2, and also reported that NaB enhances p21 expression levels in vivo. These previous studies were consistent with these results that the expression levels of p21 were decreased by high cholesterol and recovered by NaB, and p21/Nrf2 co-localization was also increased. However, p21 is a typical cyclin-dependent kinase inhibitor, which is an apoptosis marker, but it is also reported to be an apoptosis inhibition marker (Crispi. 2012). In addition, there are studies that NaB contributes to protect neurons from cell death and adverse studies that NaB induces apoptosis in the epithelial cell line Caco-2, which thereby is controversial on the regulatory role of NaB on cell death (Bourassa et al., 2016; Ruemmele et al., 2003). Therefore, the present study demonstrated that increased cell death by high cholesterol was reduced by NaB, which indicates that increased expression levels of p21 by NaB do not induce apoptosis.

Based on these results, this study hypothesized that NaB as an HDAC inhibitor increases the expression levels of p21 via the acetylation regulation of transcription factor. Although previous studies have reported that both p53 and sp1 are critical transcription factors of p21 (Koutsodontis et al., 2001), the results showed that increased p21 levels by NaB under high cholesterol conditions are due to sp1, not p53. NaB is absorbed in the cell and acts as a histone deacetylase inhibitor, which influences activity of

transcription factors. For instances, sp1 is the transcription factor of encoded protein involved in cell differentiation, cell growth, and apoptosis (Waby et al., 2010). Although several studies have reported that sp1 acetylation increases or decreases DNA-binding affinity, which influences the encoded protein of sp1 (Kou et al., 2013; Waby et al., 2010), the data demonstrated that sp1 acetylation affects the nuclear translocation of sp1, thereby this study focused on the relationship between sp1 acetylation and the nuclear translocation. In general, many previous studies described the nuclear translocation activity of transcription factors through the phosphorylation of transcription factors (Hunter et al., 1992; Karin et al., 1995). However, the nuclear translocation of several transcription factors is known to be affected by acetylation regulation because the acetylation influences the stability of transcription factors or protein-protein interaction (Park et al., 2015). The activity of some transcription factors is increased by acetylation to increase the expression levels of the target proteins, whereas the activity of some transcription factors is reduced by acetylation (Kundumani-Sridharan et al., 2012; Thiagarajan et al., 2016; Zhao et al., 2006). However, the exact mechanisms for the regulation of nuclear translocation through acetylation regulation of transcription factors are still unknown. Although there is no report that acetylation regulation of sp1 affects sp1 migration to the nucleus in neurons, the data demonstrated that nuclear translocation

of sp1 decreased by high cholesterol was recovered by NaB and again decreased by the pretreatment of ibuprofen or C646 with NaB. Thus, these findings suggested that the nuclear translocation of sp1 is reduced under high cholesterol conditions, but NaB increases the expression levels of p21 by increasing the activity of nuclear translocation of sp1 through the regulation of sp1 acetylation, and eventually stabilizes Nrf2 by contributing to p21/Nrf2 co-localization.

Taken together, it can be said that the present study first revealed the mechanisms of the dual antioxidant effect of NaB on neuronal cells under high cholesterol conditions. In other words, this study demonstrated that NaB protects SK-N-MC cells exposed to high cholesterol environment by inhibiting ROS production or facilitating ROS elimination and ultimately prevents A β accumulation due to the increased expression levels of BACE1 caused by excessive ROS (Figure 16). Furthermore, it suggests that NaB can be a therapeutic strategic candidate to AD patients caused by obesity, because obese patients who are most likely to get AD showed reduced butyrate-producing bacteria in the microbiota composition. In conclusion, this study have shown that NaB can regulate excessive ROS in SK-N-MC cells exposed to high cholesterol environment through the reduction of NOX2 expression or the increase of the expression levels of antioxidant enzymes by enhancing Nrf2 stabilization via the p21/Nrf2 pathway.

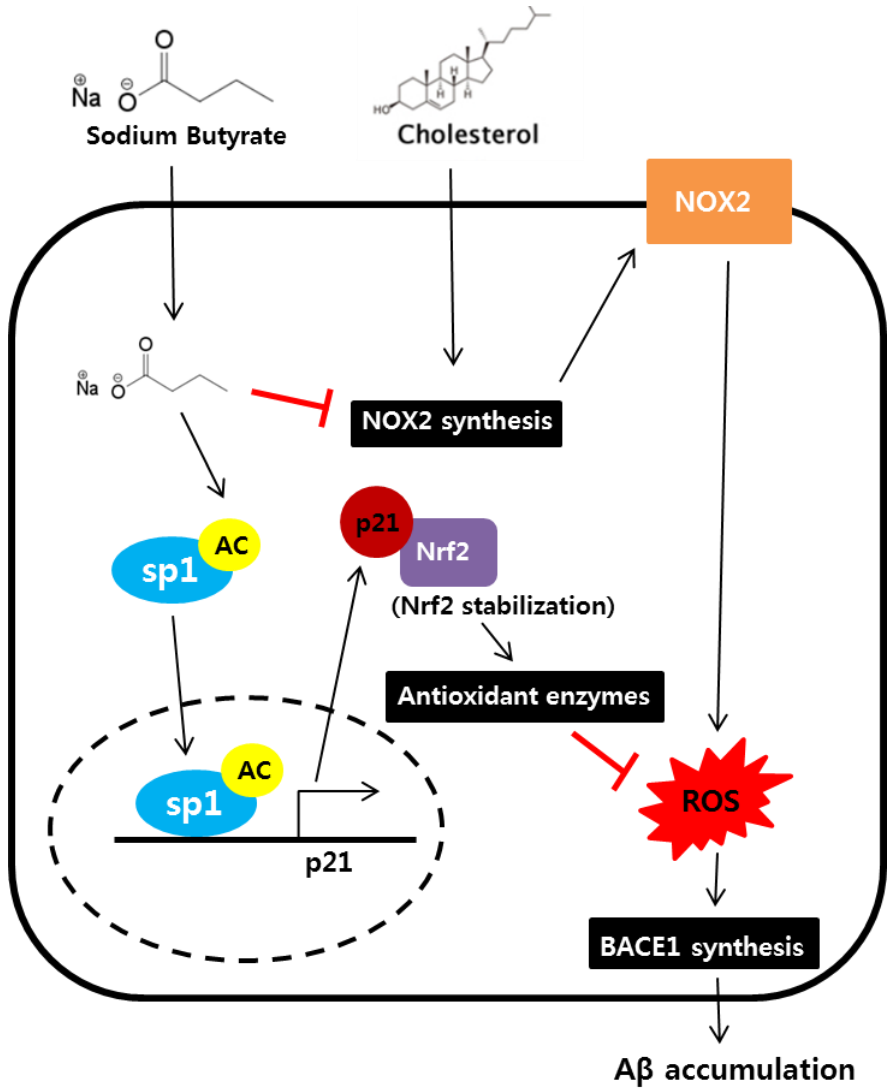

Figure 16. A hypothetical model for suppression of high cholesterol-induced ROS and Aβ accumulation by the dual antioxidant effect of NaB. Sodium butyrate (NaB) inhibits high cholesterol-induced excessive reactive oxygen species (ROS) in SK-N-MC cells through the dual antioxidant effect of NaB. NaB induces the reduction of NADPH oxidase 2 (NOX2) expression

or the increase of the expression levels of antioxidant enzymes by enhancing nuclear factor erythroid 2-related factor 2 (Nrf2) stabilization via the p21/Nrf2 pathway caused by the regulation of specifc protein 1 (sp1) acetylation (AC). NaB ultimately prevents amyloid beta peptide (Aβ) accumulation through inhibition of increased expression levels of β-site amyloid precursor protein cleaving enzyme 1 (BACE1) caused by excessive ROS.

REFERENCES

Alford, S., Patel, D., Perakakis, N., and Mantzoros, C. S. (2018). Obesity as a risk factor for Alzheimer's disease: weighing the evidence. Obes Rev 19, 269-280.

Auer, S., Rinnerthaler, M., Bischof, J., Streubel, M. K., Breitenbach-Koller, H., Geisberger, R., Aigner, E., Cadamuro, J., Richter, K., Sopjani, M., Haschke-Becher, E. T., Felder, K., and Breitenbach, M. (2017). The human NADPH oxidase, Nox4, regulates cytoskeletal organization in two cancer cell lines, HepG2 and SH-SY5Y. Front Oncol 7, 111.

Bae, Y. S., Oh, H., Rhee, S. G., and Yoo, Y. D. (2011). Regulation of reactive oxygen species generation in cell signaling. Mol Cells 32, 491-509.

Baxter, N. T., Schmidt, A. W., Venkataraman, A., Kim, K. S., Waldron, C., and Schmidt, T. M. (2019). Dynamics of human gut microbiota and short-chain fatty acids in response to dietary interventions with three fermentable fibers. mBio 10, e02566-02518.

Bolyen, E., Rideout, J. R., Dillon, M. R., Bokulich, N. A., Abnet, C. C., Al-Ghalith, G. A., Alexander, H., Alm, E. J., et al. (2019). Reproducible, interactive, scalable and extensible microbiome data science using QIIME 2. Nat Biotechnol 37, 852-857.

Bourassa, M. W., Alim, I., Bultman, S. J., and Ratan, R. R. (2016). Butyrate, neuroepigenetics and the gut microbiome: Can a high fiber diet improve brain health? Neurosci Lett 625, 56-63.

Callahan, B. J., McMurdie, P. J., Rosen, M. J., Han, A. W., Johnson, A. J., and Holmes, S. P. (2016). DADA2: High-resolution sample inference from illumina amplicon data. Nat Methods 13, 581-583.

Canani, R. B., Costanzo, M. D., Leone, L., Pedata, M., Meli, R., and Calignano, A. (2011). Potential beneficial effects of butyrate in intestinal and extraintestinal diseases. World J Gastroenterol 17, 1519-1528

Chakraborti, C. K. (2015). New-found link between microbiota and obesity. World J Gastrointest Pathophysiol 6, 110-119.

Chen, W., Sun, Z., . Wang, X. J., Jiang, T., Huang, Z., Fang, D., and Zhang, D. D. (2009). Direct interaction between Nrf2 and p21(Cip1/WAF1) upregulates the Nrf2-mediated antioxidant response. Mol Cell 34, 663-673.

Chueh, A. C., Tse, J. W., Togel, L., and Mariadason, J. M. (2015). Mechanisms of histone deacetylase inhibitor-regulated gene expression in cancer cells. Antioxid Redox Signal 23, 66-84.

Cooney, S. J., Bermudez-Sabogal, S. L., and Byrnes, K. R. (2013). Cellular and temporal expression of NADPH oxidase isotypes after brain injury. J Neuroinflammation 10, 155.

Crim, K. C., Sanders, L. M., Hong, M. Y., Taddeo, S. S., Turner, N. D., Chapkin, R. S., and Lupton, J. R. (2008). Upregulation of p21Waf1/Cip1 expression in vivo by butyrate administration can be chemoprotective or chemopromotive depending on the lipid component of the diet. Carcinogenesis 29, 1415-1420.

Crispi, S. (2012). The dual role played by p21 may influence the apoptotic or anti-apoptotic fate in cancer. J Canc Res Updates 1.

David, J. A., Rifkin, W. J., Rabbani, P. S., and Ceradini, D. J. (2017). The Nrf2/Keap1/ARE pathway and oxidative stress as a therapeutic target in type II diabetes mellitus. J Diabetes Res 2017, 4826724.

Davie, J. R. (2003). Inhibition of histone deacetylase activity by butyrate. J Nutr 133, 2485S-2493S.

Davis, M. P., Van dongen, S., Abreu-Goodger, C., Bartonicek, N., and Enright, A. J. (2013). Kraken: a set of tools for quality control and analysis of high-throughput sequence data. Methods 63, 41-49.

De la Monte, S. M., and Wands, J. R. (2006). Molecular indices of oxidative stress and mitochondrial dysfunction occur early and often progress with severity of Alzheimer's disease. J Alzheimers Dis 9, 167-181.

DeSantis, T. Z., Hugenholtz, P., Larsen, N., Rojas, M., Brodie, E. L., Keller, K., Huber, T., Dalevi, D., Hu, P., and Andersen, G. L. (2006). Greengenes, a chimera-checked 16S rRNA gene database and workbench compatible with ARB. Appl Environ Microbiol 72, 5069-5072.

Dong, W., Jia, Y., Liu, X., Zhang, H., Li, T., Huang, W., Chen, X., Wang, F., Sun, W., and Wu, H. (2017). Sodium butyrate activates Nrf2 to ameliorate diabetic nephropathy possibly via inhibition of HDAC. J Endocrinol 232, 71-83.

Duncan, S. H., Lobley G. E., Holtrop, G., Ince, J., Johnstone, A. M., Louis, P., and Flint, H. J. (2008). Human colonic microbiota associated with diet, obesity and weight loss. Int J Obes (Lond) 32, 1720-1724.

Fakhruddin, S., Alanazi, W., and Jackson, K. E. (2017). Diabetes-induced reactive oxygen species: Mechanism of their generation and role in renal injury. J Diabetes Res 2017, 8379327.

Govindarajan, N., Agis-Balboa, R. C., Walter, J., Sananbenesi, F., and Fischer, A. (2011). Sodium butyrate improves memory function in an Alzheimer's disease mouse model when administered at an advanced stage of disease progression. J Alzheimers Dis 26, 187-197.

Gustafsson, N., Culley, S., Ashdown, G., Owen, D. M., Pereira, P. M., and Henriques, R. (2016). Fast live-cell conventional fluorophore nanoscopy with ImageJ through super-resolution radial fluctuations. Nat Commun 7, 12471.

Harris, K., Kassis, A., Major, G., and Chou, C. J. (2012). Is the gut microbiota a new factor contributing to obesity and its metabolic disorders? J Obes 2012, 879151.

Hayes, J. D., and Dinkova-Kostova, A. T. (2014). The Nrf2 regulatory network provides an interface between redox and intermediary metabolism. Trends Biochem Sci 39, 199-218.

Hernandes, M. S. and L. R. Britto. (2012). NADPH oxidase and neurodegeneration. Curr Neuropharmacol 10, 321-327.

Hunter, T., and Karin, M. (1992). The regulation of transcription by phosphorylation. Cell 70, 375-387.

Jahns, F., Wilhelm, A., Jablonowski, N., Mothes, H., Greulich, K. O., and Glei, M. (2015). Butyrate modulates antioxidant enzyme expression in malignant and non-malignant human colon tissues. Mol Carcinog 54, 249-260.

Jakobsdottir, G., Xu, J., Molin, G., Ahrne, S., and Nyman, M. (2013). High-fat diet reduces the formation of butyrate, but increases succinate, inflammation, liver fat and cholesterol in rats, while dietary fibre counteracts these effects. PLoS One 8, e80476.

Karin, M., and Hunter, T. (1995). Transcriptional control by protein phosphorylation: signal transmission from the cell surface to the nucleus. Curr Biol 5, 747-757.

Kivipelto, M., and Solomon, A. (2006). Cholesterol as a risk factor for Alzheimer's disease - epidemiological evidence. Acta Neurol Scand Suppl 185, 50-57.

Klindworth, A., Pruesse, E., Schweer, T., Peplies, J., Quast, C., Horn, M., and Glockner, F. O. (2013). Evaluation of general 16S ribosomal RNA gene PCR primers for classical and next-generation sequencing-based diversity studies. Nucleic Acids Res 41, e1.

Klop, B., Elte, J. W., and Cabezas, M. C. (2013). Dyslipidemia in obesity: mechanisms and potential targets. Nutrients 5, 1218-1240.

Koutsodontis, G., Tentes, I., Papakosta, P., Moustakas, A., and Kardassis, D. (2001). Sp1 plays a critical role in the transcriptional activation of the human cyclin-dependent kinase inhibitor p21(WAF1/Cip1) gene by the p53 tumor suppressor protein. J Biol Chem 276, 29116-29125.

Kou, X. X., Hao, T., Meng, Z., Zhou, Y. H., and Gan, Y. H. (2013). Acetylated Sp1 inhibits PTEN expression through binding to PTEN core promoter and recruitment of HDAC1 and promotes cancer cell migration and invasion. Carcinogenesis 34, 58-67.

Kundumani-Sridharan, V., Van Quyen, D., Subramani, J., Singh, N. K., Chin, Y. E., and Rao, G. N. (2012). Novel interactions between NFATc1 (Nuclear Factor of Activated T cells c1) and STAT-3 (Signal Transducer and Activator of Transcription-3) mediate G protein-coupled receptor agonist, thrombin-induced biphasic expression of cyclin D1, with first phase influencing cell migration and second phase directing cell proliferation. J Biol Chem 287, 22463-22482.

Lu, Y., Fan, C., Li, P., Lu, Y., Chang, X., and Qi, K. (2016). Short chain fatty acids prevent high-fat-diet-induced obesity in mice by regulating G protein-coupled receptors and gut microbiota. Sci Rep 6, 37589.

Manea, S. A., Constantin, A., Manda, G., Sasson, S., and Manea, A. (2015). Regulation of NOX enzymes expression in vascular pathophysiology: Focusing on transcription factors and epigenetic mechanisms. Redox Biol 5, 358-366.

Martin, M. (2011). CUTADAPT removes adapter sequences from high-throughput sequencing reads. EMBnet.j 17.

Matough, F. A., Budin, S. B., Hamid, Z. A., Alwahaibi, N., and Mohamed, J. (2012). The role of oxidative stress and antioxidants in diabetic complications. Sultan Qaboos Univ Med J 12, 5-18.

Nayernia, Z., Jaquet, V., and Krause, K. H. (2014). New insights on NOX enzymes in the central nervous system. Antioxid Redox Signal 20, 2815-2837.

Park, J. M., Jo, S. H., Kim, M. Y., Kim, T. H., and Ahn, Y. H. (2015). Role of transcription factor acetylation in the regulation of metabolic homeostasis. Protein Cell 6, 804-813.

Parks, D. H., Tyson, G. W., Hugenholtz, P., and Beiko, R. G. (2014). STAMP: statistical analysis of taxonomic and functional profiles. Bioinformatics 30, 3123-3124.

Ruemmele, F. M., Schwartz, S., Seidman, E. G., Dionne, S., Levy, E., and Lentze, M. J. (2003). Butyrate induced Caco-2 cell apoptosis is mediated via the mitochondrial pathway. Gut 52, 94-100.

Silva, L. G., Ferguson, B. S., Avila, A. S., and Faciola, A. P. (2018). Sodium propionate and sodium butyrate effects on HDAC activity, histone acetylation, and inflammatory gene expression in bovine mammary epithelial cells. J Anim Sci 96, 5244-5252.

Skoglund, J. (2016). Quantification of short chain fatty acids in serum and plasma. Unpublished bachelor's thesis, http://urn.kb.se/resolve?urn=urn:nbn:se:slu:epsilon-s-6102, Swedish University of Agricultural Sciences, Sweden.

Sun, J. H., Yu, J. T., and Tan, L. (2015). The role of cholesterol metabolism in Alzheimer's disease. Mol Neurobiol 51, 947-965.

Thiagarajan, D., Vedantham, S., Ananthakrishnan, R., Schmidt, A. M., and Ramasamy, R. (2016). Mechanisms of transcription factor acetylation and consequences in hearts. Biochim Biophys Acta 1862, 2221-2231.

Waby, J. S., Chirakkal, H., Yu, C., Griffiths, G. J., Benson, R. S., Bingle, C. D., and Corfe, B. M. (2010). Sp1 acetylation is associated with loss of DNA binding at promoters associated with cell cycle arrest and cell death in a colon cell line. Mol Cancer 9, 275.

Waheed Roomi, M., Kalinovsky, T., Roomi, N. W., Niedzwiecki, A., and Rath, M. (2013). Inhibition of the SK-N-MC human neuroblastoma cell line in vivo and in vitro by a novel nutrient mixture. Oncol Rep 29, 1714-1720.

Wang, C., Li, P., Xuan, J., Zhu, C., Liu, J., Shan, L., Du, Q., Ren, Y., and Ye, J. (2017). Cholesterol enhances colorectal cancer progression via ROS elevation and MAPK signaling pathway activation. Cell Physiol Biochem 42, 729-742.

Xu, K., Dai, X. L., Huang, H. C., and Jiang, Z. F. (2011). Targeting HDACs: A promising therapy for Alzheimer's disease. Oxid Med Cell Longev 2011, 143269.

Zhang, Q. G., Laird, M. D., Han, D., Nguyen, K., Scott, E., Dong, Y., Dhandapani, K. M., and Brann, D. W. (2012). Critical role of NADPH oxidase in neuronal oxidative damage and microglia activation following traumatic brain injury. PLoS One 7, e34504.

Zhao, L. J., Subramanian, T., Zhou, Y., and Chinnadurai, G. (2006). Acetylation by p300 regulates nuclear localization and function of the transcriptional corepressor CtBP2. J Biol Chem 281, 4183-4189.

국 문 초 록

신경세포에서 부티르산에 의한 NOX2 억제와 Nrf2 안정화를 통한 고콜레스테롤 유도성 아밀로이드 생성 억제 효과

서울대학교 대학원

수의학과 수의생명과학 전공

김 서 일

지도교수 한 호 재

장내 미생물 총 조성의 불균형은 많은 비만환자에서 발생되며, 부티르산 생성균의 감소가 이에 포함된다. 부티르산은 알츠하이머병의 잠재적인 치료 전략 물질로서 오래 전부터 주목받았지만, 비만에 의해 유도되는 알츠하이머병에서 부티르산이 신경세포 내 어떤 신호 전달 경로로 아밀로이드 생성에 영향을 주는지에 대한 연구는 부족하다. 따라서 이 연구는 고콜레스테롤 환경에 노출된 신경세포에서 부티르산이 아밀로이드 생성에 미치는 영향과 기전을 규명하기 위해 수행되었다. 결과는 아래와 같다.

비만 쥐의 장내 미생물의 다양성이 일반 쥐보다 크게 감소되었고, 또한 비만 쥐의 혈장 내 부티르산 농도가 일반 쥐보다 감소되었다. 고콜레스테롤 환경에 노출된 SK-N-MC 세포에서는 NOX2 발현 증가로 활성산소종이 과생성되었으며, 부티르산은 고콜레스테롤 의해 증가된 NOX2 발현을 억제시킴으로써 활성산소종 생성을 감소시켰다. 이를 통해 궁극적으로 부티르산이 고콜레스테롤 처리에 의해 증가된 BACE1 발현과 Aβ 축적을 감소시켰다. 또한 부티르산은 sp1의 아세틸화 조절을 통하여 sp1의 핵내 이동을 증가시킴으로써 p21의 발현을 증가시켰다. 이러한 p21의 발현 증가는 p21과 Nrf2의 결합 증가 (co-localization)를 통해 Nrf2의 안정화에 크게 기여하였다. 즉, SK-N-MC 세포에서 고콜레스테롤 처리는 Nrf2의 핵내 이동을 감소시켰고, 부티르산은 Nrf2의 안정화를 통하여 Nrf2 핵내 이동을 증가시켰다.

결론적으로 고콜레스테롤 환경에 노출된 신경세포에서 부티르산은 NOX2 발현을 억제시킴으로써 활성산소종 생성을 감소시켰으며, p21과 Nrf2 결합을 증가시킴으로써 Nrf2 안정화를 통한 항산화 효소 증가로 과생성된 활성산소 종을 감소시켰다. 이를 통해 신경세포에서 부티르산은 고콜레스테롤에 의해 유도되는 아밀로이드 생성을 억제시켰다.

주요어: 부티르산, 신경세포, 아밀로이드 생성, 콜레스테롤, 활성산소종
학번: 2017-29949